Reverse genetic analysis of gene *Pp1s148_40v6* in *Physcomitrella patens*: An *AtMAX2* orthologue?

by

Ruan Morné de Villiers

Thesis presented in fulfilment of the requirements for the degree of Master of Science in the Faculty of AgriSciences at Stellenbosch University

Supervisor: Dr Paul N Hills

Co-supervisor: Prof Jens M Kossmann

March 2015

Declaration

By submitting this thesis electronically, I declare that the entirety of the work contained therein is my own, original work, that I am the sole author thereof (save to the extent explicitly otherwise stated), that reproduction and publication thereof by Stellenbosch University will not infringe any third party rights and that I have not previously in its entirety or in part submitted it for obtaining any qualification.

Ruan Morné de Villiers

December 2014

Abstract

The plant metabolite, strigolactone, has recently gained the status of phytohormone as the result of several studies that implicated its role in plant architecture. These studies would characteristically rely on the use of mutants, such as the *rms* lines that were generated in peas, that shared several characteristics. This method allowed for the identification of several genetic component of the shared pathway. It is now known that the biosynthesis of strigolactone is dependent on the sequential action of an isomerase (*D27*) and two carotenoid cleavage deoxygenases (*CCD7* and *CCD8*). Furthermore, it is known that strigolactone perception is localised to the plant nucleus, where it interacts with an α/β-fold hydrolase (D14) which would concomitantly binds to target proteins. The F box protein (*MAX2*) is able to recognize this proteïen complex. Through a *MAX2* dependent mechanism the target protein becomes tagged for proteolysis. However, this model, though intricate, has only really been shown in higher plants.

The model bryophyte, *Physcomitrella patens*, serves as a useful tool in genetic studies due to its predisposition for homologous recombination. More recently it has also gained interest in studies pertaining to strigolactones, which has led to the generation of a *Ppccd8Δ* mutant. Compared to the wild type, the *Ppccd8Δ* line produces more protonemal tissue. Furthermore, exogenous strigolactones have also been shown to inhibit colony expansion.

Here we shown that there is only a single candidate gene, *PpMAX2*, present in the *P. patens* genome that could serve as a homologue for the *Arabidopsis thaliana MAX2*. Furthermore, we show that a recombinant GFP:PpMAX2 localises to the nucleus of *P. patens* cells. A *Ppmax2::* mutant was generated which, unexpectedly, did not show the phenotype of Ppccd8Δ. *Ppmax2::* has an apparent inability to produce protonema and appears to rather dedicate its growth to the production of gametophores. A double mutant, *Ppccd8Δ max2Δ* was generated which also displayed the characteristic phenotype of *Ppmax2::*. It seems therefore that the activity of *PpMAX2* is able to override that of *PpCCD8*. By employing a GUS reporter system, we showed that the promoter, P_{PpMAX2}, is predominantly active within gametophore tissues. Taken together, these results suggest that the activity of *PpMAX2* facilitates the transition of gametophore tissue to protonema tissue.

Although exogenous strigolactones did not appear to affect the growth of the *Ppmax2::* line as it did the PpWT or *Ppccd8Δ* lines, those responses that have been ascribed to strigolactones to date have mostly been observed in protonemal tissue. We therefore suspect that any strigolactone response that might have been elicited in *Ppmax2::* would have been masked by its phenotype of predominantly protonemal tissue. We are therefore hesitant to make any sweeping statements in regards to the role *PpMAX2* might have in strigolactone perception in *P. patens*. However, though we suspect that *PpMAX2* might not be a true functional homologue for the characterised *MAX2* homologues from higher plants, we suspect that it may well be the ancestral predecessor of *MAX2*.

Opsomming

Strigolaktoon is ‘n metaboliet wat deur plante vervaardig word en is redelik onlangs as ’n fitohormoon geklassifiseer. Die klasifikasie as fitohormoon is die gevolg van verskeie studies wat strigolaktoon se rol in die plantstruktuur beklemtoon het. In hierdie studie is daar gebruik gemaak van mutante, soos onderandere die *rms* lyne, wat gegenereer is in ertjies, wat verskeie kenmerke deel. Sodoende is verskeie komponente van ’n gedeelde molekulêre padweg geïdentifiseer. Daar word tans verstaan dat die sintese van strigolaktoon afhanklik is van die stapsgewyse aksies van ’n isomerase (*D27*) en twee karotenoïedklewingsdeoksigenases (*CCD7* en *CCD8*). Verder is dit bekend dat strigolaktoon waargeneem word in die plant nukleus deur te assosieer met ’n α/β-vou-hidrolase (*D14*) wat vervolgens met teikenproteïene bind. Die kompleks word deur ’n F-boks proteïen (*MAX2*) herken wat daartoe lei dat die teikenproteïen gemerk word vir proteolise; altans, dit is tans die model wat vir hoër plante aanvaar word.

Die model briofiet, *Physcomitrella patens*, word dikwels aangewend in genetiese studies weens dit ’n hoër vatbaarheid vir homoloë rekombinasie het. Om *P. patens* te benut in navorsing wat die rol van strigolaktoon ondersoek is ook voordelig, aangesien daar reeds ’n *Ppccd8Δ* mutant beskikbaar is. In vergelyking met die wilde tipe, produseer *Ppccd8Δ* meer protonemale weefsel en blyk dit dat strigolaktoon die vermoë het om kolonie verspreiding te bekamp.

Hier wys ons dat daar ’n enkele kandidaat geen, *PpMAX2*, in die genoom van die *P. patens* teenwoordig is wat as ’n homoloog vir die *Arabidopsis thaliana MAX2* kan dien. Verder wys ons dat ’n rekombinante GFP:PpMAX2 proteïen wel na die selkern van *P. patens* selle lokaliseer. ’n *Ppmax2::* mutant is gegenereer wat, onverwags, nie die fenotipe van *Ppccd8Δ* vertoon het nie. *Ppmax2::* het ’n onvermoë om protonema te produseer en wy groei eerder aan die produksie van gametofiete. ’n Dubbele mutant, *Ppccd8Δ max2Δ*, is gegenereer wat ook die fenotipe van *Ppmax2::* vertoon het; dus kom ons tot die gevolgtrekking dat die aktiwiteit van *PpMAX2* dié van *PpCCD8* oorheers. Deur gebruik te maak van ’n GUS verklikkersisteem kon ons aflei dat die aktiwiteit van die P_{PpMAX2} promotor hoofsaaklik tot die uitdrukking van *PpMAX2* in gametofiet weefsel lei. Dit is moontlik dat die aktiwiteit *PpMAX2* dus die oorgang van gametofoor weefsel na protonema weefsel te weg bring.

Alhoewel strigolaktoon nie die groei van die *Ppmax2::* lyn beïnvloed soos vir die PpWT of *Ppccd8Δ* lyne nie, vermoed ons dat die reaksie slegs in die protonemale weefsel waargeneem sal word. Daar kan tans nie met absolute sekerheid gesê word of *PpMAX2* enigsins verbonde met strigolaktoon persepsie in mos is nie, tog vermoed ons dat *PpMAX2* ’n primitiewe voorloper vir die gekarakteriseerde *MAX2* homoloë van die hoër plante is.

Acknowledgements

This study relied on the contributions of a number of people, be that in the form of a donation, guidance, tutoring or enjoyable company. It is therefore an absolute pleasure for me to extend my gratitude to the following persons or organisations.

To Prof Mark Estelle and Dr Michael Prigge from the UCSD Division of Biological Sciences at the Howard Hughes Medical Institute, for kindly donating the pMP1335 and pMP1300 plasmids that proved invaluable in this study.

To Prof Catherine Rameau and Dr Sandrine Bonhomme, for supplying the wild-type and *Ppccd8Δ Physcomitrella patens* strains used in study.

To the National Research Foundation for funding this study.

To Rozanne Adams, Dumisile Lumkwana and Lize Engelbrecht, for patiently assisting me at the Cell Imaging Unit at the Central Analytical Facility. The results are beautiful.

To Dr Cobus Zwiegelaar and Dr Ebrahim Samodien for lending their eyes during my write-up.

To Dr James Lloyd, Dr Shaun Peters, Dr Christell van der Vyver, Dr Inonge Mulako and Dr Stanton Hector, for their inputs and advice for the tenure of this study.

To Jonathan Jewell, Zanele Mdodana, Emily Stander, Clara Conza, Anké Wiese, Déhan Dempers, Bianke Loedolff, Kyle Willard, Dineo Selebalo and all other co-workers at the Institute for Plant Biotechnology, for their friendships, assistances and advices. It's far more rewarding to study an island than to be one in science.

To Dr Bénédicte Lebouteiller, for inspiring this study.

To Prof Jens Kossmann, for providing me the opportunity to become an independent researcher.

To Daniel, Clara and my family, for keeping me distracted long enough to still love my work.

And lastly, to my brilliant supervisor, Dr Paul Hills, for giving me the freedom to pursue my ideas and allowing me to discover. I can only hope to be half as good a mentor someday.

Contents

List of Figures and Tables

List of Abbreviations and non-SI units

× *g*	gravitational acceleration
AM	arbuscular mycorrhizal
AA	amino acid
Amp	ampicillin
bp	base pair
Cm	chloramphenicol
EDTA	ethylenediaminetetraacetic acid
GtR	geneticin/G418 resistance
HygR	hygromycin resistance
Hyg	hygromycin
IAA	indole-3-acetic acid
Kan	kanamycin
LB	Luria broth
LC-MS/MS	liquid chromatography tandem mass spectrometry
LLR	leucine-rich repeat
M	molar
MES	2-[*N*-morpholino]ethanesulfonic acid
MMM	Mannitol; MES; $MgCl_2$
NMR	nuclear magnetic resonance
OE-PCR	overlap extension polymerase chain reaction
PEG	polyethylene glycol
rpm	revolutions per minute
RT-qPCR	quantitative reverse transcription polymerase chain reaction
SDS	sodium dodecyl sulphate
Spc	spectinomycin
sqRT-PCR	semiquantitative reverse-transcription polymerase chain reaction
Str	streptomycin
TAIR	The Arabidopsis Information Resource
Torr	1 Torr = 133.3 pascal
Tris	tris(hydroxymethyl)aminomethane
WT	wild type

Introduction

A brief introduction to strigolactones

For a long time it has been known that parasitic plants display host-specificity in regards to germination. This host-specificity can range from a single species to multiple species, depending on the parasite concerned. Investigations into this phenomenon led to the suspicion that a specific germination stimulant had to be responsible. While it was known that certain pure sugars could stimulate the germination of *Striga lutea*, an additional component, with properties unlike those of sugars, was believed to be at work (Brown et al., 1951; Brown et al., 1952; Worsham et al., 1964). This stimulant, simply referred to as *Striga* factor, was isolated by Cook et al. (1966) in crystalline form from the root exudates of cotton. The purified compound, named strigol, proved to be a potent germination stimulant for the root parasite, *S. lutea*, even though cotton is not a host for *S. lutea*. Strigol shares the molecular formula $C_{19}H_{22}O_6$ with gibberellic acid (GA), however, GA is not a germination stimulant of *S. lutea*, dismissing it as the potential stimulant (Cook et al., 1966). NMR and X-ray crystallography of the crystalline strigol determined that it was a terpenoid lactone (Cook et al., 1972), a group of compounds that had steadily been gaining interest for their growth regulating abilities (Gross, 1975). The potency of strigol and related compounds, together with the ubiquitous presence of similar stimulants among land plants, led to early speculation that it could represent a new class of phytohormones (Cook et al., 1972).

The earliest obstacle for strigol-related research was the difficulty in acquiring strigol from natural sources. Even though strigol has germination stimulatory activity at concentrations as low as 10^{-11} M (Cook et al., 1972), early extraction procedures required the preparation of up to 40 L of root exudate solution to deliver a mere 200 mg of crude extract (Brown et al., 1949). Furthermore, the extracted compound was not very stable, losing activity after only 72 hours at room temperature (Brown et al., 1949). A more reliable method of obtaining strigol was therefore sought through chemical synthesis. In 1974, Heather et al. were the first to describe a method for the chemical synthesis of strigol, using the structure of strigol as described by Cook et al. (1972) to guide them. Additional routes for syntheses and improvements on those efforts led to methods for producing gram quantities of (+)-strigol, the natural strigol isomer (MacAlpine et al., 1974; Dolby and Hanson, 1976; Heather et al., 1976).

With the structure of strigol determined and the optimised methods for its synthesis established, research shifted to related compounds with potential as germination stimulants for root parasites. By pre-emptively germinating parasitic weeds using a synthetic stimulatory

compound, crop farmers could potentially eliminate the weeds before they sowed their crops. The key was to find a stable, yet potent stimulant that would be cost-effective and easy to synthesise (Johnson et al., 1981). A simpler form of strigol could be a good candidate; however, would the sum of the parts prove greater than the whole? Johnson et al. (1976) showed that simple monocyclic butenolides, representing the D-ring component of strigol (*see* Fig. 1), only moderately promoted germination of *Orobanche ramosa*, but had no effect on *S. hermonthica*. However, when an enol-ether bridge (5'C-3C) bound the butenolides to a lactone moiety (ABC-ring), a significant increase in germination was observed in both species (Johnson et al., 1976). The enol-ether bridge did not, however, stimulate germination by itself and germination by precursors of the lactone moiety was only achieved in one instance (Pepperman et al., 1982). Therefore, taking into account that the individual components of strigol were not as effective at stimulating parasitic weed germination as strigol or its chemical analogues, focus shifted to the creation and use of simpler analogues of strigol that would be easier and/or more cost effective to synthesise.

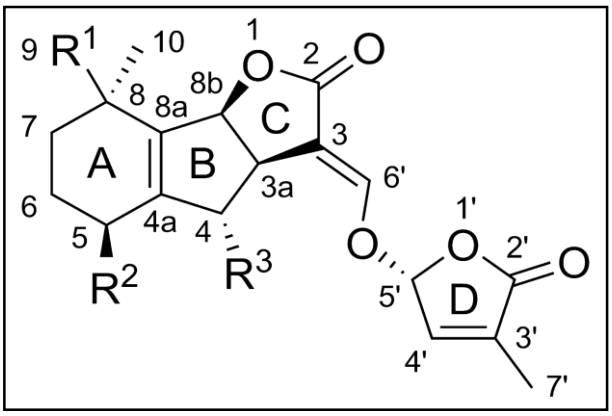

Figure 1. The general chemical structure of strigolactones with an annotation of the numerical annotation scheme commonly used. From: [http://en.wikipedia.org/wiki/Strigolactone], accessed 15 November 2014

In their inspection of the strigol structure, Johnson et al. (1976) synthesised two new strigol analogues: the two-ring butenolide-(V) (*otherwise* 2-RAS) and the 3-ring butenolide-(VII) (*otherwise* 3-RAS or GR7). Both compounds proved effective germination stimulants of *S. hermonthica* and *O. ramosa*. It was later demonstrated that GR7 was, in fact, a mixture of diasteomeric racemates, designated 3-RAS(HM) and 3-RAS(LM), of which the 3-RAS(LM) diasteoromer was shown to be the more active form for *Striga asiatica* germination trials (Pepperman et al., 1982). The continued search for the next best parasitic weed germinant led to the discovery of another racemic compound, the four-ring bis-lactone, GR24 (Johnson et al., 1981). Both GR7 and GR24 proved effective enough to warrant field trials: their

molecules are less complex and subsequently they have fewer steps in their synthesis than strigol; they are more stable than strigol under soil conditions; and they act as germination stimulants for a range of parasitic weed plants, including *S. hermonthica, S. asiatica, Orobanche* spp. and *Alectra vogellii* (Johnson et al., 1981). The characteristics of GR24 made it favourable for commercial and academic research use, spurring on the development of an improved GR24 synthesis protocol (Mangnus et al., 1992).

Though strigol and its natural analogue, epistrigol, were the first compounds isolated with potent stimulatory capabilities for parasitic weeds, sorgolactone would be the first natural analogue to be isolated from a genuine host species: *Sorghum bicolor* (Hauck et al., 1992). Apart from the above-mentioned examples, since its discovery in 1966, several additional compounds related to strigol have been found. Consequently, the word *strigolactones* was proposed as a collective name for *Striga* germination stimulants and related compounds that were generally considered to be sesquiterpene lactones (Butler, 1994).

While much progress had been made on the chemistry of strigolactones, the low concentration at which they were produced remained an obstacle in the study of their biogenesis. Subsequently, the use of radioactive isotopes as precursors to their biogenesis was therefore not considered to be feasible. As an alternative strategy, Matusova and Rani (2005) decided to rather perform a relative quantification of the strigolactones produced by plants treated with several biosynthetic inhibitors and mutant plants of the pathways speculated to produce the precursors needed for strigolactone biosynthesis. They found that fluridone, a specific inhibitor of the carotenoid biosynthesis pathway (Bartels and Watson, 1978), had the ability to reduce the germination of *S. hermonthica* by inhibiting the biosynthesis of strigolactones in cowpea, sorghum and maize. Furthermore, root exudates collected from maize mutant lines that were defective in certain steps of carotenoid biosynthesis, were also less effective at germinating *S. hermonthica* than the wild type (WT) counterparts. From these results, Matusova and Rani deduced that strigolactone was not derived from farnesyl diphosphate, as would be expected of a true sesquiterpene, but rather, that strigolactones are carotenoid derivatives.

Strigolactones and fungi

Regardless of the efficacy of strigol and its natural or synthetic analogues at stimulating the germination of parasitic weeds and notwithstanding the promise initial trial experiments held for its commercial application in parasitic weed control, a reasonable explanation for why plants were producing these compounds - seemingly to their own detriment - was still

needed. A possible answer to this question was found by studying a second type of symbiosis to which plants have committed themselves.

Mycorrhizae are the symbiotic associations between the roots of plants and the mycelia of mycorrhizal fungi. The association typically involves the extraction of nutrients from soil by the fungi in exchange for carbohydrates from the autotrophic plant host. The vesicular arbuscular mycorrhizal (AM fungi) fungi are a monophyletic clade of fungi that were assigned their own phylum, *Glomeromycota*, based on molecular, morphological and ecological evidence (Schüßler et al., 2001), making them distinct from the other known mycorrhiza-forming fungal species. They may not be as rich in species numbers or as diverse as other fungal lineages, however, being the most wide-spread of the mycorrhizal fungi, these obligate symbionts make up the majority of all mycorrhizal associations and are therefore invaluable in terms of economy and ecology (Brundrett, 2002).

The AM fungi associate with the roots of plants, forming vesicles and arbuscules to facilitate the movement of nutrients between their hosts and themselves. An arbuscule refers specifically to the haustorium formed between mutualists and, in the case of AM fungi, it is represented by the fungal hypha that penetrates the cell wall (though not the cell membrane). Within the cell wall the hypha undergoes extreme branching until a tree-like structure (hence ‘arbuscule’) is formed.

A specific sequence of developmental steps are followed during the formation of the haustorium from a fungal spore or a hypha, and chemical signals from the host plants play a key role in guiding this process. In 2005, Akiyama et al. set out to identify the specific compound(s) that cause the extreme branching that typically gives rise to the arbuscules. Previous attempts at identifying branching factors for AM mycorrhizal fungi experienced obstacles that were quite similar to those experienced in the earlier searches for the *Striga* germination factors, namely the low concentration at which the compound was being exuded by roots (Tamasloukht et al., 2003) and its relative instability (Akiyama et al., 2005). After isolating measurable quantities of the compound from *Lotus japonicus* root exudate solution and subjecting the branching factor to spectroscopic analysis and chemical synthesis, Akiyama et al. (2005) found that the branching factor was indeed a strigolactone: 5-deoxy-strigol. Finally, strigolactones had a functional role for plants. What still remained to be identified was the molecular pathways for strigolactone biosynthesis and perception in plants.

The highly-branched peas

Plant growth and development is a tightly regulated process. The hormones produced by plants (phytohormones) are a main component of this regulation. While the effects of phytohormones can be apparent even on an organismal level, it is by understanding their mechanics at a cellular and subcellular level that we truly gain insight into how they work. Nevertheless, plants that display phenotypes that reflect aberrations of molecular pathways serve as useful tools for gaining insight into the roles of the various components of those pathways.

In 1994, Beveridge et al. began the description of pea (*Pisum sativum*) cv. Torsdag lines from an ethyl methanesulfonate-mutagenized library. The recessive mutations of the *ramosus* (Lat., "*branched*") lines *rms1*, *rms2*, *rms3*, *rms4* and *rms5* all led to severely branched phenotypes, hinting to a lack of apical dominance. Auxin-cytokinin balance is known to play a role in maintaining apical dominance (Napoli et al., 1999; Leyser, 2003), however, when the levels of the auxin indole-3-acetic acid (IAA) were measured for all lines and compared to WT it was found that the auxin homeostasis had not been negatively affected, but rather, that IAA had even been upregulated in the cases of *rms1* (Beveridge et al., 1997a) and *rms2* (Beveridge et al., 1994). Grafting combinations of scions and rootstocks of the various lines was carried out to discern putative roles for the genes affected. While branching inhibition was recovered by grafting the *rms1*, *rms2*, *rms3* (partially) and *rms5* scions onto a WT rootstock, the *rms4* mutant scion remained unaffected (Beveridge et al., 1994; Beveridge et al., 1996; Beveridge et al., 1997a; Morris and Turnbull, 2001). Taken together these results suggested that unknown branching factors, synthesised in the roots and capable of being translocated across the grafts, had an influence on branching. The *RMS2* and *RMS3* loci were initially speculated to encode for genes involved in the biosynthesis of these unknown branching factors (Beveridge et al., 1996), however, a more comprehensive grafting study would later directly implicate the *RMS1* and *RMS5* loci in the generation of this signal. The locus *RMS4* was assigned a putative role in the perception of the transmissible signal (Beveridge et al., 1996; Beveridge et al., 1997b). Because the *rms2* and *rms3* mutant genotypes were able to complement each other and restore the branching to a WT state following reciprocal grafts, it was suspected that two independent branching factors, of which one was presumed to be cytokinin, could be involved in the root-derived shoot inhibition (Beveridge et al., 1996).

To gain insight into the speculated hormonal aberrations that underlie the *rms* phenotypes, cytokinin levels of the *rms1* line, as well as reciprocal grafts of the *rms4* and WT lines were measured. Grafting of *rms4* shoots consistently caused an approximately 40-fold decrease

in the cytokinin levels in the xylem sap of rootstocks compared to WT shoots, regardless of the rootstocks' genotype. This would indicate that the *RMS4* locus, acting from the shoot, has a role in dictating the cytokinin export from the roots (Beveridge et al., 1997b). Knowing that IAA levels in the shoots of the *rms4* line were not altered, auxin suppression of cytokinin production was ruled out as a potential mechanism (Beveridge et al., 1996; Beveridge et al., 1997b). Furthermore, the *rms1* mutation resulted not only in a decrease of root xylem cytokinin levels, but also a small, yet significant, increase in shoot IAA levels (Beveridge et al., 1997a).Therefore, the results of the *RAMOSUS* studies together with previous works (Hosokawa et al., 1990), provided ample evidence that apical dominance was not merely dictated by the shoot apex or auxin/cytokinin ratios within dormant tissues, but that another underlying mechanism had to be involved. However, though auxin may not have proven the primary determinant of axillary bud outgrowth, the *RMS1* dependent signal was shown to at least partly rely on an auxin signal to relieve bud dormancy (Beveridge et al., 2000), giving evidence that a balance of different hormones was still at play, rather than a model where a single signal would override the functions of all other factors involved.

The long-lived *Arabidopsis*

Senescence in plants is a process that basically entails controlled aging: plants are able to determine, to an extent, the rate at which certain tissues need to age and the use this "awareness" to redistribute nutrients from these foreordained tissues to the rest of the plant. In an attempt to gain greater insight into the genetic components that govern this process, Oh et al. (1997) isolated plants displaying a delayed senescence phenotype from a pool of EMS-subjected *Arabidopsis thaliana* Colombia-0 plants. The line *oresara9* (oresara meaning 'long living') did not only display a delay in the onset of several phenotypes that typically characterise senescence, such as the of chlorophyll content, the retention of photochemical efficiency and Rubisco activity, and the onset of senescence associated RNase and peroxidase activity, but also responded in a normal (WT-like) manner to the known senescence-associated phytohormones: abscisic acid, methyl jasmonate and ethylene (Oh et al., 1997). Even though *ore9* satisfied all the phenotypic requirements to credit its delayed senescence, the phenotype of the mutant was quite distinct from the other lines studied (Oh et al., 1997). Mapping and concomitant sequencing of the *ORE9* locus revealed that it encodes for a 693-amino acid F-box protein (Woo et al., 2001).

The highly branched *more axillary growth (max1* through *max5*) mutants, that, like the described *rms* mutants of *P. sativum*, displayed an inability to repress growth from leaf axils, were also isolated from *A. thaliana* backgrounds (Stirnberg et al., 2002). Mapping and

cloning of the *max2* mutation revealed it to be at the same locus as *ore9* (Stirnberg et al., 2002). The *max1* and *max2* mutants were both described as bushy, however, this evidenced bushiness was ascribed to outgrowth of axillary shoots from buds confined to the basal shoots and not to those located in the higher shoots or inflorescence (Stirnberg et al., 2002). Grafting experiments of *max1*, *max3* and *max4* scions onto WT rootstocks demonstrated, as was observed in the grafting studies for *rms1*, *rms2* , *rms3* and *rms5*, that a graft transmissible signal, apparently active from the roots, was responsible for inhibiting branching in the shoots (Turnbull et al., 2002; Sorefan and Booker, 2003). Mapping, cloning and sequencing would further demonstrate that the *MAX* and *RMS* genes are part of a conserved pathway in controlling shoot branching: *MAX3* and *RMS5* were found to be homologues, both encoding for orthologues of the carotenoid cleavage dioxygenase (CCD), CCD7 (Booker et al., 2004; Johnson et al., 2006); *MAX4* and *RMS1* are orthologues, encoding for another CCD, CCD8 (Sorefan and Booker, 2003); and *MAX2* and *RMS4* were found to be orthologues for the same F-box protein .

The CCDs are a family of proteins from *A. thaliana* that were grouped together on the basis of their sequence similarity (Schwartz et al., 2004). While, at the time, the exact enzymatic functions of CCD7 and CCD8 were not known, Booker et al. (2004) speculated that CCD7 and CCD8 had to be involved in the modification of carotenoids to produce the signal that was apparently absent from the *max3* and *max4* mutants. Results from Booker et al. (2004) showed that CCD7 cleaved carotenoids to produce apocarotenoids, prompting Schwartz et al. (2004) to follow up on these findings with a more rigorous biochemical characterization of the CCD7 and CCD8 enzymes. To this end, the CCD7 enzyme was expressed in a β-carotene-overexpressing *Escherichia coli* line, pACBETA. The pACBETA line develops an orange colour due to the accumulation of β-carotene, however, expression of CCD7 led to a significantly reduced accumulation of this carotenoid, yielding yellow, rather than orange colonies (*see* fig.1 *A*; (Schwartz et al., 2004). Moreover, biochemical analysis revealed that an apocarotenoid, 10'-apo-β-carotenal was produced as a consequence of the specific cleavage of the C9-C10 double bond of β-carotene (Schwartz et al., 2004). By co-expression of the CCD7 and CCD8 enzymes, it was shown that CCD8 catalyses the subsequent step in the synthesis of the branching signal by cleaving the CCD7 by-product, 10'-apo-β-carotenal, at the C13-C14 double bond, to produce the ketone, 13-apo-10-β-carotenone (Schwartz et al., 2004). This enzymatic pathway, initially characterised using AtMAX3 and AtMAX4, was subsequently shown to be conserved in other species, e.g. pea, petunia and rice (Alder et al., 2008). The evidence for a carotenoid-derived hormone signal was steadily mounting, models for its role in shoot branching were becoming more defined, and yet the signal responsible remained elusive (Ongaro and Leyser, 2008).

The convergence of research concerning strigolactones, phytobranching and AM fungi

In 2008 two research groups simultaneously presented the ground-breaking discovery that would connect strigolactone research to research of the elusive branching inhibition signal. Using the knowledge that both strigolactones and the branching signals are carotenoid-derived and that both act with high impact, yet at low doses, Gomez-Roldan et al. and Umehara et al. showed that strigolactones were in fact phytohormones with roles in the regulating shoot branching.

The first evidence was provided using the known action of strigolactones on AM fungi (Akiyama et al., 2005). Root exudates of the pea mutants *rms1* and *rms5*, the CCD8 and CCD7 defective mutants respectively, could not induce hyphal branching of *Gigaspora rosea* and *G. gigantea* to the same extent as WT pea (Gomez-Roldan et al., 2008). Similarly, root exudates of *rms1* were not as effective at stimulating germination of the parasitic weed *Orobanche crenata* as WT pea (Gomez-Roldan et al., 2008). Together these findings gave indirect evidence for a reduced production of strigolactones by the *rms1* and *rms5* mutants. Consequently, it would indicate that both the shoot multiplication signal and strigolactones are carotenoid derivatives that share some part of the pathway downstream of the CCD7- and CCD8-mediated cleavage of carotenoids. To gain more direct evidence for these findings, Gomez-Roldan et al. (2008) carried out liquid chromatography/tandem mass spectrometry on root exudate samples of the *rms1* and *rms4* and WT pea lines. They detected orobanchyl acetate and another uncharacterised strigolactone in the samples of both the WT and the *rms4* lines, however, they were not able to detect these compounds in the extract from *rms1*, implicating CCD8 directly in the biosynthesis of strigolactone.

To test whether strigolactone was in fact the signal that controls branching in pea by inhibiting lateral bud outgrowth, the synthetic strigolactone, GR24, was applied directly to the axillary buds of the pea *rms1* and *rms4* lines (Gomez-Roldan et al., 2008). Application of GR24 did indeed inhibit the outgrowth of axillary buds for the *rms1* line. Its failure to inhibit the outgrowth of buds on *rms4* was also in agreement with the theory that the F-box protein encoded for by *rms4* was implicated in the detection and downstream signalling of the branching factor.

Umehara et al. (2008) chose rice as the model for their study using the *dwarf* mutant lines that had known orthology to particular pea *rms* and *Arabidopsis max* lines. Quantification using liquid chromatography quadruple/time-of-flight tandem mass spectrometry was

performed on extracts of rice root exudates and of endogenous strigolactones. For the lines *d17* (*ccd7*) and *d10* (*ccd8*), strigolactones were consistently reduced under normal and phosphate deficient conditions. By contrast, strigolactones of the *d3* (F-box) line were comparable to WT under standard conditions and up-regulated under inorganic phosphate deficiency, hinting at a role for D3 in a speculated feedback mechanism for control of strigolactone levels. Direct treatment of the *d17*, *d10*, *d3* and WT lines with GR24 and the natural strigolactones (+)-strigol and (+)-5-deoxy strigol was performed in a hydroponic system to gather direct evidence for strigolactone control of tiller outgrowth. As was expected, the *d17* and *d10* lines showed responsiveness to the strigolactones, with near-complete inhibition of tiller bud outgrowth for seedlings treated with 1 µM GR24. By contrast, *d3* failed to respond to the treatments, consistent with its role as a putative signalling component.

Both studies also looked at the role of strigolactones in *Arabidopsis*, particularly in the *max* lines. While the Gomez-Roldan et al. study applied GR24 directly to axillary buds and leaf axils, Umehara et al. opted for a hydroponic system where seedlings were treated through the hydroponic solution. Ultimately the conclusions for both *Arabidopsis* experiments were the same and indicated that the shoot multiplication signal responsible for branching inhibition in *Arabidopsis* was a carotenoid-derived strigolactone(s) that is generated through the expression of the *MAX1, MAX3* and *MAX4* loci; furthermore, that the downstream signalling of strigolactone was dependant on the F-box protein, MAX2. Taken together, enough evidence had been provided to propose strigolactones as the long-elusive phytohormone that had a major part to play in controlling higher plant architecture.

The strigolactone pathway: a more complete picture

A number of naturally occurring strigolactones have been described (*see* Fig. 2), and the strigolactones of natural origin are strikingly similar on a molecular level, hinting either at a common origin for their biosynthesis or a conformity enforced on them by the perception components of the hormone pathway. The answer is probably a bit of both: it is known that the characterised strigolactones are in fact synthesised from a common mobile precursor (Alder et al., 2012), and a number of authors have speculated as to how the different isoforms could be related (Rani et al., 2008; Xie et al., 2010; Kohlen, 2011); yet, it has also been demonstrated that parasitic weed seed germination can be stimulated by the use of synthetic strigol analogues and related natural sesquiterpene lactones (Johnson et al., 1976; Pepperman et al., 1982; Macías et al., 2006).

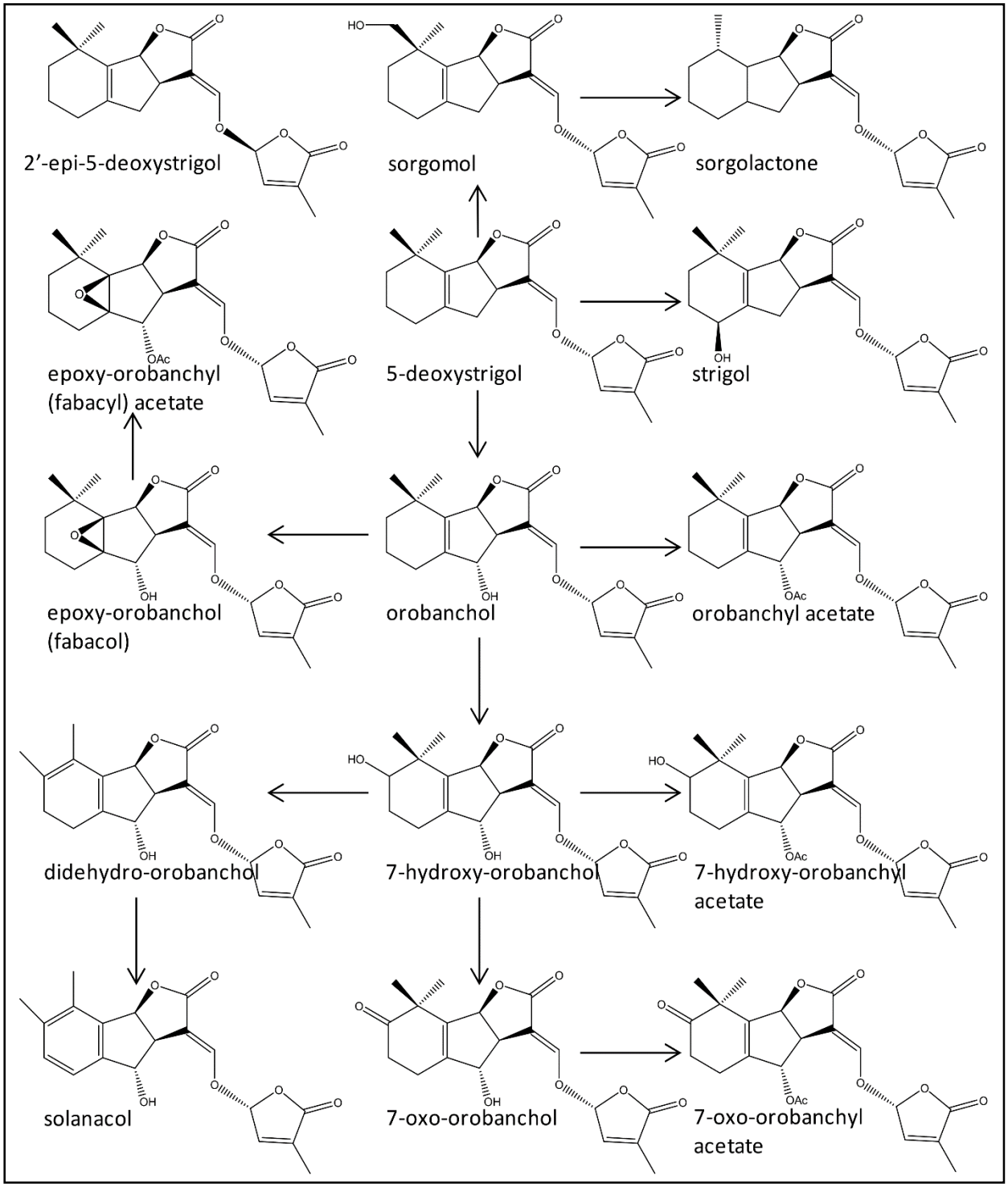

Figure 2. The postulated pathway of strigolactone modification starting from 4-deoxystrigol. From Kohlen (2011)

Strigolactones are derived from carotenoids, therefore they are apocarotenoids (Schwartz et al., 2004; Matusova and Rani, 2005). Although the link between research of strigolactones and of the shoot multiplication signal had not been drawn at the time, Schwartz et al. (2004) had begun their initial description of a putative biosynthesis pathway for the shoot multiplication signal using their knowledge of its most probable substrate (β-carotene) and of the participation of the enzymes, CCD7 and CCD8. By expression of the enzymes, individually and in combination, in a β-carotene over-expressing *E. coli* line, they were able to deduce putative mechanisms for the enzymes. However, a notable drawback of their study was that the enzymes were characterised by expression in an all-*trans*-β-carotene overexpressing *E. coli* line. Alder et al. (2012) would later demonstrate that the substrate for CCD7 is in fact 9-cis-β-10'-carotenal, the isomerization product of D27. D27, a carotene isomerase, converts all-*trans*-β-carotene (C_{40}) to 9-cis-β-carotene (C_{40}) through all-*trans*/9-*cis*-β-carotene activity (Lin et al., 2009; Alder et al., 2012; Waters et al., 2012a). Subsequently, 9-cis-β-carotene is cleaved by CCD7 at the C9'-C10' double bond to yield the aldehyde 9-*cis*-β-apo-10'-carotenal (C_{27}) and β-ionone (C_{13}) (Alder et al., 2012). CCD8 primarily uses the C_{27}-aldehyde to yield carlactone, a C_{19} precursor of strigolactone, although it is also capable of catalysing a much slower reaction whereby all-*trans*-β-apo-10'-carotenal (C_{27}) is converted to β-apo-13-carotenone (C_{18}) (Alder et al., 2012; Seto et al., 2014). Although no direct evidence has been obtained to show how carlactones are converted to biologically active strigolactones, Scaffidi et al. (2013) showed that the mechanism is at least partially dependant on the functions of the cytochrome P450, MAX1. By feeding ^{13}C-labelled carlactone to the CCD8 defective rice mutant, *d10*, it was shown that the (11*R*)-isotope of carlactone gets converted to the strigolactone (-)-2'-*epi*-5-deoxystrigol (Seto et al., 2014). However, a study of two rice *MAX1* orthologues from rice demonstrated that the diversity of endogenous strigolactones could probably not be attributed to the MAX1 catalysis alone, as the products of the two *MAX1* loci caused up or down regulation of all strigolactones - not just specific strigolactone species (Cardoso et al., 2014). Studies of crop cultivars producing lower levels of strigolactones, such as those by Satish et al. (2012), hold promise for the identification of more genes involved in either strigolactone biosynthesis, or in the regulation thereof.

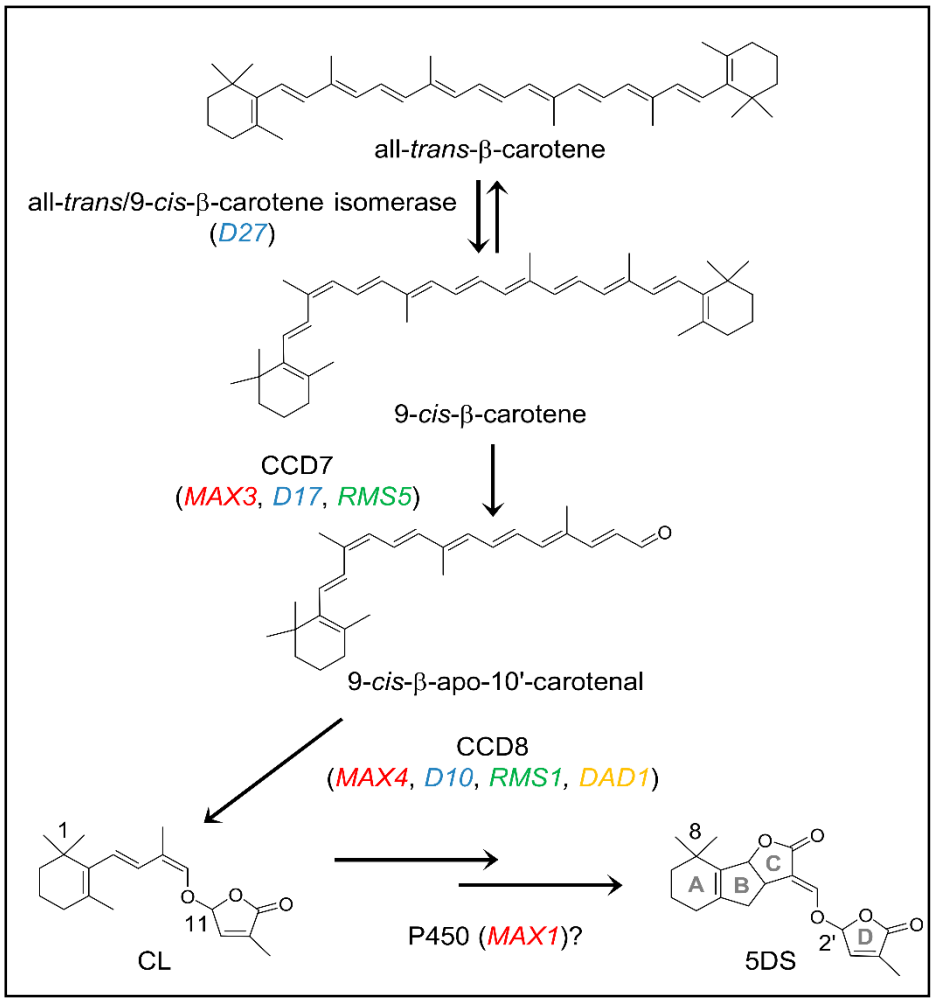

Figure 3. The pathway for strigolactone biosynthesis from all-*trans*-β-carotene. From Seto et al. (2014).

The mechanism by which strigolactones are perceived has also received a lot of attention, and although the entire mechanism has not yet been clarified, definite components thereof have been resolved. An α/β-fold hydrolase, D14, interacts directly with strigolactones as the primary strigolactone preceptor in the pathway (Arite et al., 2009; Gaiji et al., 2012; Hamiaux et al., 2012; Zhou et al., 2013). The strigolactone docks within the substrate binding pocket of D14, where a catalytic triad consisting of asparagine, histidine and serine residues is found This leads to a nucleophilic attack of the strigolactone molecule by the 97th serine residue (S97) of D14 (Zhao et al., 2013). The resulting electron shift causes the enol ether bridge connecting the ABC-tricyclic lactone and D-ring butenolide of the strigolactones to break, leading to the hydrolysis of targeted strigolactones. The S97 residue stabilises the D-lactone by-product, until it takes up a reactive water molecule to the yield the reaction intermediate, 2,2,4-trihydroxy-3-methyl-3-butenal (Zhao et al., 2013). Intramolecular

rearrangement leads to the formation of an unstable butenolide, which, upon subsequent dehydration, yields a hydroxy D-ring (Nakamura et al., 2013; Zhou et al., 2013). This hydroxy D-ring is proposed to act as the effector molecule that allows D14 to destabilise (Hamiaux et al., 2012; Nakamura et al., 2013; Zhao et al., 2013). The relaxed form of D14 is able to bind proteins that act as repressors of the strigolactone pathway, such as the class I Clp ATPase, D53 (Jiang et al., 2013; Zhou et al., 2013) or the DELLA protein, SLR1 (Nakamura et al., 2013). The D14/repressor complex interacts with the rice F-box protein, D3 (MAX2). F-box proteins such as D3/MAX2/RMS4 characteristically have both an F-box domain and a leucine-rich repeat (LRR) domain. The LRR domain of the F-box protein interacts with the target protein; in the case of D3, it is assumed that the LRR domain interacts with the D14/repressor-complex (Zhou et al., 2013; Koltai, 2014), though the stereochemistry of this binding will need clarification, if not validation. Most F-box proteins are also presumed to form part of Skp, Cullin, F-box (SCF)-E2 containing complexes. The SCF-complex would target a protein, through polyubiquitination, to the ubiquitin-26S proteasome (Vierstra, 2009). In concurrence with this model, a strigolactone-dependant, F-box mediated degradation of D14 in *A. thaliana* (Chevalier et al., 2014) and D53 in rice (Zhou et al., 2013) has been observed.

Introducing *Physcomitrella patens*

Studies of branching have mostly been confined to the larger vascular organisms, such as *Arabidopsis*, pea, petunia and rice. For strigolactone research this has proved very fruitful thus far, however, there is a potential to overlook important mechanisms that could, potentially, only be observable in simpler model organisms. Additionally, by studying a complex regulatory mechanism in (supposedly) less complex organisms, one could simplify the model of its regulation and gain insight into the evolution of said mechanism. A natural interest in the role of strigolactones in simpler model organisms was therefore pursued once a basic model for its pathways had been established (Gomez-Roldan et al., 2008). The bryophyte, *Physcomitrella patens*, proved a most amenable model for this purpose.

The moss *P. patens* has a number of attributes that makes it a useful model plant. Firstly, it has the ability to complete its entire lifecycle *in vitro* by growing on a minimal medium of sterile soil, sand or agar containing simple salts in only two months (Wettstein, 1924; Engel, 1968; Nakosteen and Hughes, 1978). Another attractive feature of *P. patens* is that it has a lifecycle dominated by a haploid gametophyte stage (Wettstein, 1924; Rensing et al., 2008) allowing the phenotypes associated with recessive traits to manifest perceptibly. By means of apospory or protoplast fusion, one could also determine the dominance of traits in a

simplified manner (Engel, 1968; Grimsley et al., 1977a; Grimsley et al., 1977b). The most attractive feature *P. patens* for modern molecular biologist has to be that, of all studied plants, it has the highest frequency of homologous recombination (Schaefer and Zrÿd, 1997). This allows a researcher to circumvent the tedious screening and selection methods required to identify mutants in other plants, by generating a construct to recombine with targeted loci. In combination with the availability of the complete genome sequence (Rensing et al., 2008), this liberates studies of specific gene functions from the crippling dependence on mutant libraries. Classical hormones such as auxin and cytokinin are also conserved in *P. patens* (Cove et al., 1990; Cove and Knight, 1993), along with major components of the strigolactone pathway, including homologues for several characterised genes known to partake in the pathway (Gomez-Roldan et al., 2008; Proust et al., 2011; Delaux et al., 2012) and the ability to synthesise and respond to strigolactones (Proust et al., 2011; Hoffmann et al., 2014). Due to major differences in the morphologies of bryophytes and other embryophytes, the hormones might not influence plant organs in the same way, however, components of their respective molecular pathways maintain a level of conservation to those found in higher plants (Prigge et al., 2010), probably due to the specific ways in which proteins, genetic elements and/or metabolites interact.

To understand the value of *P. patens* as a model plant for strigolactone research, one also has to take into account specific differences between bryophytes and vascular plants. The first distinction should certainly be made on a morphological level. Considered from the haploid spore, the lifecycle of *P. patens* is initiated by the germination of the unicellular spore, which can be characterised by the emergence of the germ tube (Nakosteen and Hughes, 1978). The germ-tube is rich in chloroplasts and gives rise to the first type of protonema through apical division: the primary chloronema (Allsopp and Mitra, 1958; Ashton et al., 1979). Chloronemal cells grow relatively slow and are characterised by their abundance of round chloroplasts (Schmiedel and Schnepf, 1980; Cove et al., 1990). They have the potential to divide subapically to give rise to new apices within the protonema's filamentous structure. The second tissue-type composing the protonema is the caulonema (Sironval, 1947; Allsopp and Mitra, 1958). Caulonemal cells differentiate from apical chloronemal cells and are distinguished as being longer and thinner, with fewer spindle-shaped chloroplasts (Allsopp and Mitra, 1958). Subapical division of caulonemal cells could give rise to more protonemal filaments, or they could differentiate to form gametophore buds (Allsopp and Mitra, 1958). Gametophores are the leafy-shoot structures that grow from these buds. They have defined organs, including the stems, leafs and rhizoids. Under low temperature and short day-length conditions, the sexual organs, the antheridia and archegonia, also develop from the leafy shot to produce gametes (Engel, 1968; Nakosteen

and Hughes, 1978; Hohe et al., 2002). When water is available, the motile, haploid sperm cells, developed within an antheridium, make their way to the archegonia. Within the archegonia, the haploid egg cells await the sperm cells for fertilisation, which results in the formation of the diploid zygote. The zygote develops into an embryo, which matures into the sporophyte. The sporophyte of *P. patens* is shorter than other studies moss species (e.g. *Funaria hygrometrica*, *Physcomitrium pyriforme*, *Bryum caespiticium* and *Ceratodon purpureus*) due to its notably shorter setum (Wettstein, 1924). A spore capsule, carried upon the setum, generates new haploid spores, completing the life-cycle (Wettstein, 1924; Reski, 1998).

Strigolactones in *P. patens*

The first study to consider the role of strigolactones in bryophytes was executed by Proust et al. (2011) who characterised the *CCD8* homologue in *P. patens*. The *PpCCD8* gene was found to be differentially expressed at the bases of gametophores. Furthermore, the strigolactones orobanchyl acetate, fabacyl acetate, 7α-hydroxyorobanchyl acetate, 7-oxoorobanchyl acetate, orobanchol and strigol were found to be the major strigolactones produced by *P. patens*. A knock-out mutant for the *CCD8* locus, *Ppccd8Δ*, was generated and its strigolactones were measured. No orobanchyl acetate, fabacyl acetate or orobanchol could be measured, however, only a minor decrease in in 7-ocxoorobanchyl acetate was found. A slight increase in strigol was also measured along with small quantities of 5-deoxy strigol, which was not detected in the WT. Both the WT and the *Ppccd8Δ* mutants displayed strigolactone responsiveness upon exogenous GR24 application. Moreover, distinctive differences observed in the phenotypes between the WT and *Ppccd8Δ* mutants also gave strong evidence of roles for endogenous strigolactones in *P. patens* growth regulation. The first such role is in the control of lateral branching from subapical protonemal cells: the *Ppccd8Δ* mutant produces significantly more subapical branches than its WT counterpart. Another significant difference between WT and *Ppccd8Δ* was its unchecked colony expansion: three weeks after spore germination, WT *P. patens* colony expansion becomes reduced, however, this is not the case for the *Ppccd8Δ* line, which continued to expand without restraint. It was therefore speculated that a role for strigolactone could also be to control *P. patens* colony expansion and, indeed, it was demonstrated that exogenous strigolactones, in the form of GR24 or produced by a proximate WT colony, could regulate the expansion of the *Ppccd8Δ* line. (Proust et al., 2011)

In a follow-up study of the phenotypic aberrations resulting from the *Ppccd8* mutation, Hoffmann et al. (2014) demonstrated that growth of caulonemata of *P. patens* is affected by

strigolactones: for the *Ppccd8Δ* line, a significant increase in the rate of cell division accompanied with a slight increase in cell length was measured compared to WT or strigolactone-treated *Ppccd8Δ*. This resulted in longer caulonemal filament. The number of caulonemal filaments was also increased, however, this might be attributed to the increase in chloronemal branching, as was found in the Proust et al. (2011) study.

Rationale

The generation of the *Ppccd8Δ* mutant has given insight into the role of endogenous strigolactones in *P. patens*, however, homologues for several other components of strigolactone signalling, originally discovered within angiosperms, have either not yet been characterised or are entirely unaccounted for in bryophytes (Delaux et al., 2012; Waters et al., 2012b; Challis et al., 2013). We have therefore set out to determine whether the closest *P. patens* homolog of the MAX2 F-box protein plays a role in strigolactone signalling in moss, to determine whether this protein and, concomitantly, the molecular pathway delineated by strigolactones, is conserved among land plants.

Materials and Methods

P. patens culture

Methods and materials employed for the culture of *P. patens* were essentially as described by Collier and Hughes (1982) and Cove et al. (2009). The strain used as WT was the Gransden strain (Engel, 1968). The Ppccd8Δ strain, kindly supplied to our laboratory by Prof C Rameau and Dr S Bonhomme, was also derived from the Gransden strain (Proust et al., 2011).

Standard *P. patens* growth conditions

For the standard growth conditions, moss cultures were maintained in a temperature-controlled growth room at a set temperature of 25 ± 2°C. A 16/8 hour light/dark photoperiod was maintained using cool white fluorescent lights (50 µM photons m^{-2} s^{-1}; OSRAM L 58W/640, Germany).

Solutions and culture media for *P. patens*

For *P. patens* culture, variations of Knop medium were used. Stock solutions of macronutrient salts were prepared at 100× strength, and a solution of micronutrients/trace elements was prepared at 1000× strength (Table 1). Reagents B, C, D, G, T and $CaCl_2$ were prepared as aqueous solutions, autoclaved and stored at -20°C. The $FeSO_4$ reagent was always prepared as a fresh aqueous solution.

Table 1. Components of media for *P. patens* culture

			Concentration			
Reagent	Strength	Component	Stock		Final	
B	100 ×	$MgSO_4$	0.1	M	1	mM
C	100 ×	KH_2PO_4	184	mM	1.84	mM
D	100 ×	KNO_3	1	M	10	mM
G	100 ×	$C_4H_{12}N_2O_6$	0.5	M	5	mM
T	1000 ×	H_3BO_3	9.93	mM	9.93	µM
		$Na_2MoO_4 \cdot 2H_2O$	0.103	mM	0.103	µM
		$CoCl_2 \cdot 6H_2O$	0.266	mM	0.266	µM
		$ZnSO_4 \cdot 7H_2O$	0.191	mM	0.191	µM
		$MnCl_2 \cdot 4H_2O$	1.97	mM	1.97	µM
		KI	0.169	mM	0.169	µM
		$CuSO_4$	0.22	mM	0.22	µM
		$Al_2(SO_4)_3 \cdot 18H_2O$	0.57	mM	0.57	µM
$CaCl_2$	100 ×	$CaCl_2$	1	M	1	mM
$FeSO_4$	1000 ×	$FeSO_4$	45	mM	45	µM

Liquid culture medium:

Reagents B, C, D and T (and, where explicitly mentioned, also reagent G) were diluted to 1× concentrations in dH_2O. The pH of the medium was adjusted to 5.8 with KOH before it was autoclaved. After autoclaving, the correct amounts of $CaCl_2$ and $FeSO_4$ reagents were filter sterilised (0.22 µm) directly into the medium.

Solid culture medium:

Liquid culture medium was solidified with agar (Sigma-Aldrich®, USA-MO), which was added to a final concentration of 0.55% (w/v) after the pH of the medium was adjusted.

Sporophytogenesis medium:

Reagents B, C and T were diluted to 1× concentration and solution D was added to a final concentration of 0.04× (400 µM). Agar was added to a final concentration of 0.55% (w/v) before the pH of the medium was adjusted to 5.8. The medium was autoclaved, after which $CaCl_2$ and $FeSO_4$ solutions were directly filter-sterilised (0.22 µm) to the medium to final concentrations of 1× each.

Routine culture

Routine subculture of the *P. patens* lines was conducted to generate tissue for experimental applications. The method simply entails that moss colonies be divided and grown, and was preferred to grinding and plating out, as it allows one to detect and avoid possible contamination before it affects downstream applications.

For routine subculture, tissue culture plates, filled with 30 to 40 mL of solidified BCDT or BCDGT, were prepared. BCDT sufficed for most experiments, however, due to their stunted protonemal growth, BCDGT medium, supplemented with extra nitrogen as di-ammonium tartrate (reagent G), was preferred for the *Ppmax2::* lines. Antibiotics (G418 or hygromycin B) were added to cool, unsolidified medium before pouring plates as required. Tissue from established plates was collected using sterile forceps, separated, and pressed onto the surface of the freshly prepared plates. Routinely, five freshly spotted colonies were grown per plate. Plates were sealed with Micropore™ surgical tape (3M™, USA-MN) and placed under standard growth conditions.

Culture on Cellophane overlaid plates

For applications that required large amounts of protonemal tissue, the use of cellophane disks overlaid onto the gel medium allows for easy collection of tissue. Solid BCDGT medium was preferred over BCDT, as it favoured and sped up the growth of protonemal tissue.

Tissue culture plates were prepared with solid 30 to 40 mL BCDGT medium and allowed to solidify. An autoclaved 325P cellophane disk (A.A. Packaging Limited, UK) was placed on top of the medium and allowed to hydrate for 5 min. The hydrated disks were flattened out over the surface of the media. Tissue was collected from isolated uncontaminated colonies and added to a sterile ULTRA TURRAX® dispenser tube (IKA®, Germany). Tissue from plates with isolated colonies was preferred and plates entirely covered in protonema were avoided to prevent carryover of contamination. Autoclave-sterilised water was added to the tube driver (2 mL per plate to be generated plus an additional 5 mL). The dispenser tubes were then sealed and fitted to a ULTRA TURRAX® tube driver (IKA®, Germany). The tissue was homogenised by blending for 10 to 20 seconds. Blended tissue was poured into a 50 mL tube. The blended tissue was plated out by pipetting 2 mL of homogenate per cellophane-overlaid plate using a 5 mL pipette fitted with a cut 5 mL tip. Cut tips were preferred as the apertures of uncut tips were too small and would get clogged by the homogenate. The plates were sealed with surgical tape and placed under standard growth conditions.

GR24 treatment

Culture plates filled with 40 mL of solid BCDGT medium, supplemented with GR24 to a final concentration 10^{-6} M were prepared. GR24 stocks were prepared at 10^{-4} M in 10% (v/v) acetone, therefore, control BCDGT plates were supplemented with 0.1% (v/v) acetone. The solidified medium was overlaid with a cellophane disk over which 3 mL of solid BCDGT was cast and set. Colonies of the lines PpWT, *Ppccd8Δ* and *Ppmax2::* were spotted onto the plates. Plates were sealed with surgical tape and placed under standard growth conditions for 40 days. Fresh plates were prepared every 7th day for disks to be transferred to fresh medium to avoid GR24 depletion.

Transformation of *P. patens*

A new transformation protocol was established by modifying methods from Cove et al. (2009), Hoffmann and Charlot (2009) and Liu and Vidali (2011). The modified method was developed not only to accommodate for the equipment at our disposal, but it potentially increased the chances for *Ppmax2::* and *Ppccd8Δ max2Δ* mutant protoplasts to regenerate.

Solution and culture media used for transformations

PRM-L:

D-mannitol was added to liquid culture medium, containing reagent G, to a final concentration of 8.5% (w/v) before the pH of the medium was adjusted.

PRM-T:

D-mannitol was added to a concentration of 8% (w/v), and agar to a concentration of 0.4% (w/v) to liquid culture medium containing reagent G before the pH was adjusted.

PRM-B:

D-mannitol was added to a concentration of 6% (w/v), and agar to a concentration of 0.55% (w/v) to liquid culture medium containing reagent G before the pH was adjusted.

Driselase solution:

A 2% driselase solution was prepared by dissolving 1 g of driselase (Sigma-Aldrich®) in 50 mL of 8.5% (w/v) D-mannitol solution. The resulting mixture was centrifuged at 10 000 ×*g* for 10 min at 4 °C. The supernatant was filter-sterilised (0.22 µm) directly into sterile 10 mL tubes to prevent continuous freezing and thawing of its comprising enzymes. The aliquots were stored at -20 °C and used as described below.

MMM solution:

MMM solution was composed of 8.5% (w/v) D-mannitol, 0.1% (w/v) 2-(*N*-morpholino)ethanesulfonic acid and 15mM $MgCl_2$ combined as an aqueous solution. After dissolving all the components, the solution was filter sterilised and stored at -20°C until needed.

PEG solution:

The aqueous PEG solution was freshly prepared on the day of each transformation. For 10 mL of solution, 4 g of polyethylene glycol (MW 4000) powder was weighed out and melted in a microwave. In a separate tube, 0.7 g of D-mannitol and 236 mg of $Ca(NO_3)_2$ were weighed out and dissolved in 100 µL of 1M Tris-HCl (pH 7.2) and a minimal amount of dH_2O. This mannitol solution was combined with the melted PEG and the total volume brought to 10 mL with dH_2O. The solution was filter-sterilised with a 0.22 µm filter. The final solution thus contained 7% (w/v) D-mannitol, 100 mM $Ca(NO_3)_2$, 10 mM Tris-HCl (pH 7.2) and 40% (w/v) PEG4000.

Isolation of protoplasts

Four cellophane overlaid plates with ground tissue of a particular line were prepared for each transformation. After 7 days of regeneration, the tissue was collected and added to a sterile, detergent-free, foil-covered 500 mL beaker. Ten millilitres of PRM-L was then added to the beaker and mixed thoroughly to break up all tissue clumps. Ten millilitres of driselase solution was added to the mixture to degrade the cell walls. The beaker was incubated on a rocker set at 15 rpm at room temperature to release the protoplasts. After 60 minutes, the mixture was filtered through a 100 µm cell strainer (BD Falcon™, 08-771-19) into a 50 mL collection tube. An additional 5 mL of PRM-L was used to rinse the beaker and also filtered through the cell strainer.

The protoplasts were sedimented and the supernatant was removed. The sedimented protoplasts were gently resuspended, firstly in 1 mL of PRM-L and then to a total of 15 mL of PRM-L. The mixture was again sedimented and the supernatant was removed. The protoplasts were resuspended firstly in 1 mL of PRM-L and then in an additional 9 mL of PRM-L. The total number of protoplasts in the 10 mL mixture was quantified from a 40 µL aliquot using a Neubauer-improved bright-line counting chamber (0.100 mm depth, 0.0025 mm^2 volume; Marienfeld-Superior, Germany). The remaining mixture was sedimented and the supernatant removed. The protoplasts were resuspended in MMM solution to a final concentration of 1.6 million protoplasts/mL. All sedimentation steps were

carried out at room temperature, by centrifuging the mixtures at 150 ×*g* for 5 min without breaks.

PEG-mediated transformation

A prepared solution of approximately 60 µg of linearised construct DNA in a maximum volume of 50 µL was added to the bottom of a 10 mL culture tube for every transformation. By using a pipette fitted with a cut 1 mL tip, 600 µL of MMM-resuspended protoplasts was added to the DNA. Generally, by following the protoplast isolation protocol, enough protoplasts were yielded for four or more transformations, however, a single mock transformation, for which construct DNA was excluded, was also carried out as a control. Lastly, 700 µL of PEG solution was added to complete the mixture. The tubes were gently tapped or swirled to mix the contents. The tubes were left at room temperature for 30 min, after which the protoplasts were heat-shocked for 5 min at 45°C by holding the tubes in a water bath. After the heat-shock, the tubes were returned to room temperature for another 30 min.

PRM-L was added to the transformed mixture in firstly 5 × 300 µL and then 5 × 1 mL aliquots, with 2 min intervals between the additions of each aliquot, resulting in a total addition of 6.5 mL of PRM-L to each transformation tube. The transformations were left overnight at room temperature in the dark to allow the protoplasts recover and to sediment under gravity.

Plating out of transformed protoplasts

For each transformation, two PRM-B culture plates were freshly prepared and overlaid with sterile cellophane disks. The volume of each of the transformed protoplast mixtures was reduced to 2 mL each by removing excess supernatant. The remaining 2 mL was gently tapped or swirled to resuspend the sedimented protoplasts, after which 2 mL of cool, yet molten, PRM-T was directly added. The 4 mL of contents was quickly mixed by pipetting and immediately plated out on the prepared PRM-B plates by pipetting 2 mL per plate. The PRM-T layer was allowed to solidify, after which the plates were sealed with surgical tape and transferred to standard *P. patens* growth conditions.

Selecting for stable transformants

After a week of regeneration at standard growth conditions, the cellophane disks bearing the regenerated colonies were transferred aseptically to freshly prepared BCDGT plates supplemented with either 35 mg/L hygromycin B (Sigma-Aldrich®) or 50 mg/L G418 (Sigma-Aldrich®). After a week of selection, most colonies without G418 resistance would be dead

and those without hygromycin B resistance would have their growth severely stunted. The disks were then transferred aseptically to BCDGT plates without any antibiotics to relieve the selective pressure that would otherwise maintain transient transformants. After 1 week on non-selective media, the disks were again transferred to selective plates. The colonies that survived the second round of selection were usually/mostly stable transformants, however, to ensure that the native locus was knocked-out or replaced by an antibiotic-resistance cassette, verification was performed through PCR.

Preparation of construct DNA for transformation

For transformation using any knock-out construct, a maximal volume of 50 µL of DNA was used and a DNA quantity of 30-60 µg was required. Therefore, a protocol that could consistently yield pure DNA at a high (>1.5 µg/µL) concentration was established by modifying steps from the plasmid isolation protocol (see *General methods* for the original protocol and solutions used).

A liquid culture of the *E. coli* strain harbouring the plasmid of interest was established by inoculating 5 mL of liquid from a single colony from a culture plate. The 5 mL culture was grown overnight at 37°C on a shaker at 200 rpm. The 5 mL liquid culture was used to inoculate a larger, 250 mL LB liquid culture for overnight growth. The 250 mL culture was divided in two batches. Each batch was pelleted in a 50 mL tube by centrifuging at 3000 ×*g* for 10 min. The supernatant was removed and the pellet was resuspended in 8.5 mL of resuspension solution. Resuspended cells were lysed by the addition of 8.5 mL of lysis solution, and the cell debris was neutralised by the addition of 12 mL of neutralisation solution. The mixture was centrifuged at 3000 ×*g* for 10 min, whereafter the supernatant was removed to a fresh 50 mL tube. Isopropanol was added to a total volume of 50 mL (approximately 21 mL or 0.7 volumes). The plasmid DNA was pelleted after 2 min of precipitation by pelleting the mixture at 3000 ×*g* for 10 min. The supernatant was removed from the pellet, whereafter the pellet was washed two times with 70% (v/v) ethanol. The pellet was air-dried and then resuspended in 100 µL dH_2O. The mixture was centrifuged for 10 min to pellet undissolved impurities. The supernatants from the two separately purified batches were combined at this stage and then divided into 5 aliquots of approximately 40 µL per aliquot. The aliquots were individually purified as PCR products using the GeneJET PCR Purification Kit (Thermo Scientific, USA-MA) according to the kit's supplied instructions, with the final elution step being performed by the addition of 30 µL of elution buffer. The DNA concentrations of the eluents yielded from the 5 respective aliquots were quantified using a NanoDrop™ Lite spectrophotometer. The DNA was subjectively combined and/or diluted at this step to deliver approximately 120 µg of DNA in 88 µL. To this was added 2 µL of a

specified restriction enzyme and 10 µL of the relevant 10× buffer. This mixture was incubated overnight at 37°C to allow for linearization of the plasmid construct, after which the reaction was terminated at 80°C for 10 min. A 1 µL aliquot of this restriction reaction was electrophoresed on an agarose gel to confirm the linearization of the plasmid. The terminated reaction was then utilised as the prepared solution of linearised construct DNA in the *PEG mediated transformation* section.

General methods

Polymerase Chain Reactions

For general PCR where the products were not required for subsequent cloning and for colony PCR from *E. coli*, GoTaq® DNA Polymerase (Promega, USA-WI) was used. Phusion High-Fidelity DNA Polymerase (Thermo Scientific) was utilized for PCRs of which the product would be used for subsequent cloning, on account of the low error-rate of the enzyme. For tissue sampling for screening purposes, a 0.5 mm Harris Uni-Core™ tissue punch was used on, preferentially, protonemal tissue, followed by direct amplification of the DNA from the *P. patens* tissue sample using the Phire Plant Direct PCR Master Mix (Thermo Scientific). For low-error rate amplification of products destined for cloning into the Gateway® entry vector pCR®8/GW/TOPO®, the Expand High Fidelity PCR System (Roche, Switzerland) was employed, as this enzyme A-tails the PCR products for cloning into T-vectors. All enzymes were utilised according to the manufacturer's instructions. Sequences for all primers used are listed in Appendix A.

Luria broth (LB):

For liquid bacterial cultures, an autoclaved mixture of 1% (w/v) bacteriological peptone, 0.5% (w/v) yeast extract and 1% (w/v) NaCl was used. For bacterial culture on solidified medium, 1.5% (w/v) bacteriological agar was added to the mixture before autoclaving. Antibiotics were added to the LB media as is described in specific methods, using the convention x^n to describe the addition of specific antibiotics at specified concentrations, where *x* is an abbreviation of the antibiotic used (*see* List of abbreviations), and *n* is the mg/L working concentration at which the antibiotic was used.

DNA manipulations

Plasmid isolation

Plasmid DNA was isolated using a miniprep protocol modified from Sambrook and Russell (2001). A 5 mL LB liquid culture of the *E. coli* strain harbouring the plasmid of interest was

inoculated from a single colony and grown overnight at 37°C on a shaker at 200 rpm. A cell pellet was generated by centrifuging the culture at 16 000 ×*g* for 5 min. The supernatant was removed and the pellet was resuspended in 250 µL of resuspension solution (50 mM Tris-HCl [pH 8.0], 10 mM EDTA, 100 µg/mL RNaseA). Cells were lysed by the addition of 250 µL of lysis solution (200 mM NaOH , 1% [w/v] SDS), whereafter the mixture was neutralised by the addition of 350 µL of neutralisation solution (3.0 M potassium acetate [pH 5.5]). The neutralised mixture was centrifuged for 5 min at 16 000 ×*g* to pellet major cellular components. The supernatant was transferred to a fresh tube to which 600 µL isopropanol was added to precipitate plasmid. Exactly 2 min was allowed for plasmid precipitation, after which the plasmid was pelleted by centrifuging the mixture at 16 000 ×*g* for 5 min. The supernatant was removed and the pellet was washed by the addition of 70% (v/v) ethanol. The plasmid pellet was recovered by centrifuging at 16 000 ×*g* for 5 min. The ethanol was removed by decanting, followed by evaporation, and the dry pellet was resuspended in dH_2O. The entire protocol was carried out at room temperature. The concentration of isolated plasmid was determined on a NanoDrop™ Lite spectrophotometer. Isolated plasmid was stored at -20°C.

PCR/DNA purification and gel extraction

For the purification of DNA generated by PCRs or by miniprep plasmid isolations, the GeneJET PCR Purification Kit (Thermo Scientific) was used according to the manufacturer's instructions. For extraction of restricted DNA fragments or PCR products from an agarose gel after separation by electrophoresis, the GeneJET Gel Extraction Kit (Thermo Scientific) was used according to the manufacturer's instructions. Only where explicitly mentioned was the GeneJET Plasmid Miniprep Kit (Thermo Scientific) used to isolate plasmid.

Restriction digestion

All restriction digestions were catalysed by using enzymes from Thermo Scientific at 1 unit per 10 µL of total reaction volume and, when necessary, the optimal buffer was selected by using the manufacturer's online tool (Thermo Scientific, http://www.thermoscientificbio.com/webtools/ doubledigest/). If the product of a digestion was intended to serve as a vector for a subsequent ligation, the digestion reaction was supplemented with 5 units of FastAP (Thermo Scientific). All restriction digestions were catalysed overnight at 37°C and terminated by incubating samples at 80 °C for 10 min.

Ligations

All ligation reactions were catalysed by use of T4 DNA Ligase of Thermo Scientific according to the manufacturer's instructions, except that all ligations were catalysed at room

temperature overnight. For ligation of blunt-ended DNAs (*Eco*32I and *Stu*I digestion products), PEG4000 (Sigma-Aldrich®) was added to a final concentration of 5% (w/v).

Heat-shock transformation

All transformations of plasmid into *E. coli* were conducted via standard heat-shock protocol (Sambrook and Russell, 2001), which entails the co-incubation of plasmid and 50 µL heat-shock competent *E. coli* cells on ice for 10 min, heat-shock in a 42°C water-bath for 45 s and then the immediate return of the heat-shocked cells to ice. A total of 350 µL of liquid LB was added to the transformed cells, whereafter they were left to regenerate in a 37°C incubator for an hour. The transformations were plated out onto 2 LB plates (200 µL per plate) supplemented with appropriate antibiotics, and colonies were allowed to grow overnight at 37°C.

Genomic DNA extraction from *P. patens*

An extraction method was established by modifying methods proposed by Edwards et al. (1991). Approximately 200 µL of *P. patens* protonemal tissue from a line of interest was scraped from a cellophane-overlaid plate and added to a 2 mL tube. To the tissue was added 2 glass beads and 400 µL of extraction buffer (200 mM Tris-HCl [pH 7.5], 25 mM EDTA, 250 mM NaCl, 0.5% [w/v] SDS).The tissue was homogenized using a vortex mixer until only a green, lump-free mixture remained. The tube was centrifuged at 16 000 ×*g* for 10 min. The supernatant was transferred to a new tube, and an equal volume of isopropanol was added to this extract to precipitate the DNA. The DNA was allowed to precipitate for 30 min at -20°C. The DNA was pelleted from the mixture by centrifuging at 16 000 ×*g* for 15 min at 4°C. The supernatant was removed and the DNA pellet was washed by adding 1 mL of 70% (v/v) ethanol. The pellet was recovered from the wash by centrifuging at 16 000 ×*g* for 10 min at room temperature. The ethanol was removed by decanting it from the tube and the DNA pellet was left to air-dry at room temperature. The dry pellet was resuspended in 50 µL dH_2O. The concentration of gDNA was quantified using a NanoDrop™ Lite spectrophotometer and the DNA was stored at -20°C.

GUS staining

To determine where the expression of recombinant β-glucoronidase was localized in the P_{PpMAX2}*:GUS* lines, a protocol of Hiwatashi et al. (2008) was modified as described below. A *GUS*-expressing mutant line was spotted on solidified BCDGT medium overlaid with a cellophane disk and grown for 3-4 weeks under standard *P. patens* growth conditions.

Approximately 5-7 mL of fresh X-Gluc substrate solution (0.5 mM X-Gluc [Thermo Scientific], 0.5 mM potassium ferrocyanide, 0.5 mM potassium ferricyanide, 0.05% [v/v] Triton X-100, 50 mM sodium dihydrogen phosphate) was added directly to the culture dish. The tissue/cellophane disk was gently agitated with a toothpick to ensure that all the tissue was submerged in the solution, yet with enough care not to disrupt the colony structure. The plate was subjected to a constant 150 Torr vacuum for 30 min at room temperature in the dark. Following the vacuum infiltration, the plate was sealed with Parafilm and incubated at 37°C in the dark for 2 days.

After incubation, the X-Gluc substrate was removed from the culture dish by pipetting, and replaced by 5-7 mL of 5% (v/v) acetic acid. The acetic acid was allowed to soak for 10 min and then removed. The tissue was washed, sequentially, with 30%, 50%, 70%, 100% and 100% (v/v) ethanol. For the ethanol wash steps, the culture dish was filled with a specific ethanol solution, starting from the weakest concentration, left at room temperature for 5 min, and emptied by pipetting. After the second 100% ethanol wash step, 5-7 mL of dH_2O was added to the culture dish to displace the ethanol. The submerged tissue was viewed under a light microscope. To observe localized *GUS* expression in individual gametophores, the gametophores were simply removed from the colony mass and placed on solidified BCDT medium.

Generating the *Ppmax2::* lines

The protein ID of *AtMAX2*, At2g42620, was identified from the ARAMEMNON 8 database by a keyword search (Schwacke et al., 2003). This identifier was used to locate the Gene Details page of AtMAX2 (http://www.phytozome.net/genePage.php?search=1&searchText=transcriptid%3A19640104&crown&method=0&detail=1, *accessed online at* www.phytozome.net *on* 2 Dec 2014) on the Phytozome version 9 database (Goodstein et al., 2011). Homologues for AtMAX2 limited to the organism *P. patens* were identified under the “Protein Homologs” tab, located on the Gene Details page, by applying a filter specific for the databases of *Arabidopsis thaliana* and *Physcomitrella patens v1.6*. From these hits, we identified the locus Pp1s148_40v6, which was subsequently designated *PpMAX2*.

Using WT *P. patens* gDNA as template and the primers PpMAX2_► and PpMAX2_◄, a 2493 bp genomic fragment, encoding for *PpMAX2*, was amplified by Phusion PCR. The PCR product was cloned directly into the pJET1.2/blunt vector using the CloneJET PCR Cloning Kit (Thermo Scientific) to generate pJET1.2/blunt::*PpMAX2*. The pJET1.2/blunt::*PpMAX2* construct was transformed into the *E. coli* strain DH5α by standard heat-shock and transformed colonies were selected for on LB Amp^{100} plates. Colonies

containing insert were screened for by colony PCR using the pJET1.2_► and the pJET1.2_◄ primers. Positive colonies were subsequently screened for orientation using pJET1.2_► and PpMAX2_◄. A colony positive for the directional screen was used to inoculate 5 mL of liquid LB Amp^{100} for overnight culture at 37°C. Plasmid was extracted from the culture using the GeneJET Plasmid Miniprep Kit and sent for sequencing using the primers pJET1.2_►, pJET1.2_◄, PpMAX2_seq►1, PpMAX2_seq►2, PpMAX2_seq►3, PpMAX2_seq◄1, PpMAX2_seq◄2 and PpMAX2_seq◄3 (see Appendix C).

More pJET1.2/blunt::PpMAX2 plasmid was isolated by the described plasmid isolation protocol. A 50 µL *Eco*32I restriction digestion was set up for 10 µg of plasmid DNA. Similarly, the GtR cassette, encoding *nptII*, from the pMBL11a plasmid and the HygR cassette, encoding *hph*, from the pMBLH8a plasmid, were liberated by *Eco*32I digestion. The restricted plasmids were run on an agarose gel to separate the fragments. The bands corresponding to the linearised pJET1.2/blunt::*PpMAX2* backbone (5290 bp) and the respective antibiotic cassettes (±1600 bp for GtR and ±1700 bp for HygR) were excised and extracted after separation by. Two ligation reactions were set up whereby the respective antibiotics were ligated to the pJET1.2/blunt::*PpMAX2* backbone. The products were transformed into *E. coli* DH5α by standard heat-shock. Transformed colonies were selected for on LB Amp^{100}. Colony PCRs and restriction mappings were performed to confirm the insertion of the antibiotic cassettes. The resulting plasmid constructs, designated p*Ppmax2-nptII*-KO1 (Appendix D) and p*Ppmax2-hph*-KO1 were linearised by *Not*I digestion and used to transform WT *P. patens* by the described transformation method. Stable mutants were screened for using either $G418^{50}$ (*nptII*-KO1 lines) or Hyg^{30} (*hph*-KO1 lines) supplemented plates. PCR screens were carried out on stable resistant lines with the PpMAX2_scr► and PpMAX2_scr◄ primers by Phire PCR. Lines that had undergone homologous recombination at the targeted locus were designated *Ppmax2::* to distinguish them as insertion or gene-disruption lines.

Generating the *Ppmax2Δ* and *Ppccd8Δ Ppmax2Δ* lines

To generate a complete knock-out mutant for the *PpMAX2* coding region, a 4686 bp amplicon of the Pp1s148_40v6 locus was amplified by Phusion PCR from *P. patens* gDNA using the PpMAX2Δ_5'► and PpMAX2Δ_3'◄ primers. This 4686 bp product was purified and used as template for two independent Phusion PCR reactions. For both reactions, only 1 ng of template was used in the 50 µL Phusion PCR reactions. The first reaction used the primers PpMAX2Δ_5'► and PpMAX2Δ_5'◄ to amplify a 1170 bp fragment (5'-*PpMAX2*) and the second reaction used the primers PpMAX2Δ_3'► and PpMAX2Δ_3'◄ to generate a 1008 bp fragment (3'-*PpMAX2*). The products were run on an agarose gel and extracted,

independently. The purified fragments served as template for an overlap-extension PCR (OE-PCR) by means of the Phusion PCR protocol. For the OE-PCR, 1 ng of each template was included in the total reaction and the primers used were PpMAX2Δ_5'► and PpMAX2Δ_3'◄ (*see* Appendix E). The 2183 bp product, named *PpMAX2*flanks, was cloned into the pJET1.2/blunt vector using the CloneJET PCR Cloning Kit. The pJET1.2::*PpMAX2*flanks construct was transformed into *E. coli* DH5α. Amp^{100}-resistant colonies were screened by colony PCR using the pJET1.2_► and pJET1.2_◄ primers and purified plasmid from a single positive colony was submitted for bidirectional sequencing using the pJET1.2 primers. The confirmed pJET1.2::*PpMAX2*flanks construct was linearised by *Stu*I restriction digestion and subsequently purified. The GtR cassette from pMBL11a and the HygR cassette from pMBLH8a were independently liberated by *Eco*32I digestion, separated by agarose gel electrophoresis and extracted. The cassettes were respectively ligated to the linearised pJET1.2::*PpMAX2*flanks DNA to yield the vectors p*Ppmax2-nptII*-KO2 (*see* Appendix F) or p*Ppmax2-hph*-KO2. These knock-out constructs were transformed into *E. coli* DH5α and selected for on Amp^{100} selective plates. Several colonies were subjected to colony PCRs using the pJET1.2_► and pJET1.2_◄ primers. Plasmids isolated from colonies that amplified ±4000 bp fragments were subjected to restriction mapping. A single construct for the GtR selectable marker was selected to transform both WT and *Ppccd8Δ P. patens* lines. Similarly, a HygR construct was also selected to transform both *P. patens* lines. For both KO2 constructs, *Not*I was used to linearise plasmid DNA prior to transformation. Stable transformants were selected for and were subsequently screened by Phire PCR using the PpMAX2_scr► and PpMAX2_scr◄ primers. The lines resulting from transformation by the KO2 constructs had the entire *PpMAX2* coding sequence displaced by the selectable-marker cassette and were therefore designated *Ppmax2Δ* to distinguish them as deletion lines.

Generating the *ZmUbi:gfp:PpMAX2* lines

Total RNA was extracted from WT *P. patens* protonemal tissue using the RNeasy® Plant Mini Kit by following the manufacturer's instructions (QIAGEN, Germany). Purified RNA was used as template for oligo$(dT)_{18}$-primed cDNA synthesis using the RevertAid™ H Minus First Strand cDNA Synthesis Kit (Thermo Scientific). The single-stranded cDNA was used as template for an Expand Hifi PCR to amplify the *PpMAX2* coding sequence by using the PpMAX2_► and PpMAX2_◄ primer set. The 2493 bp product was cloned into the pCR®8/GW/TOPO® vector using the pCR®8/GW/TOPO® TA Cloning® Kit (Life Technologies®, USA-CA) following the manufacturer's instructions. The product, pCR8::*PpMAX2*, was transformed into *E. coli* DH5α. Transformed colonies were selected for on Spc^{100} plates,

screened for insert by colony PCR using the M13_► and M13_◄ primers. Colonies that screened positive for insert were subsequently subjected to colony PCR using the M13_► and PpMAX2_◄ primers to determine the orientation of the insert. Plasmid was isolated from a single positive colony using the GeneJET Plasmid Miniprep Kit and sequenced with the primers M13_►, M13_◄, PpMAX2_seq►1, PpMAX2_seq►2, PpMAX2_seq►3, PpMAX2_seq◄1, PpMAX2_seq◄2 and PpMAX2_seq◄3.

An LR-clonase reaction was executed to recombine the pMP1335 vector (kind gift from Prof Mark Estelle and Dr Michael Prigge; http://labs.biology.ucsd.edu/estelle/Moss_files/ pK108N+Ubi-mGFP6-GW.gb) with the pCR8::*PpMAX2* construct using the Gateway® LR Clonase® Enzyme mix of (Life Technologies®) by following the manufacturer's instructions. The product, pMP1335::*PpMAX2* was transformed into *E. coli* DH5α and transformants were selected for on LB Kan^{100}. Colonies were screened by colony PCR using the Ubi-exp and PpMAX2_seq◄3 primers. Plasmid was isolated from resulting colonies and the pMP1335::*PpMAX2* construct was linearised by *Sfi*I digestion and transformed into WT *P. patens*. Lines that maintained stable resistance to G418^{50} were screened for insert by Phire PCR using the GFP_► and PpMAX2_◄ primers. For one of these positive *GFP:PpMAX2* lines the localisation of the recombinant GFP:*PpMAX2* was determined by visualising protonemal tissue on a confocal microscope (Carl Zeiss Confocal LSM 780 Elyra with SR-SIM superresolution plasform). For analysis, protonemal tissue was fixed in 4% (v/v) formaldehyde for 10 min and then stained with a 0.0125% (w/v) Hoescht33342 solution. Images captured were analysed by the ZEN 2012 (blue edition) software package (Carl Zeiss, Germany).

Generating the P_{PpMAX2}:*GUS* lines

The pMP1301 vector was modified from the pMP1300 [http://labs.biology.ucsd.edu/estelle/Moss_files/ pMP1300-K108N+Ubi-GW-GUS.gb] vector that was a gift from Prof Mark Estelle and Dr Michael Prigge. To delete the *ZmUbi-1* promoter from pMP1300, a Phusion PCR was set up using 1 ng of pMP1300 DNA as template. The primers Ubipr and Ubi-exp were used to amplify the entire vector, with the exclusion of the promoter sequence. The PCR product was ligated as a blunt-ended fragment by the described methods. The resulting product was transformed into the *ccd*B resistant *E. coli* strain DB3.1 and transformants were selected for on LB Kan^{100} Str^{50} Cm^{35} plates. Colonies were mapped using the restriction enzyme set: *Nco*I, *Nru*I, *Pst*I and *Pvu*I. Plasmid isolated from a colony that mapped as expected was named pMP1301.

To amplify the putative promoter for *PpMAX2* (P_{PpMAX2}), 1961 bp of DNA directly upstream of the *PpMAX2* start codon was amplified from *P. patens* gDNA by Phusion PCR using the

primers P_{PpMAX2}_► and P_{PpMAX2}_◄. The product was purified and subsequently cloned into the pCR®8/GW/TOPO® vector using the pCR®8/GW/TOPO® TA Cloning® Kit following the manufacturer's instructions. The product, pCR8::P_{PpMAX2} was transformed into *E. coli* DH5α. Transformants were selected for on LB Spc^{100} plates. Colonies were screened by colony PCR using the primers M13_► and M13_◄. A colony PCR using the primers M13_► and P_{PpMAX2}_◄ was carried out to discern between colonies by the orientation of their insert.

A single colony was selected that screened positive for the directional PCR. Plasmid was purified from this line using the GeneJET Plasmid Miniprep Kit and sent for sequencing using the M13_►, M13_◄, P_{PpMAX2}_seq► and P_{PpMAX2}_seq◄ primers.

An LR-clonase reaction between the pMP1301 plasmid and the pCR8::P_{PpMAX2} plasmids was set up using the Gateway® LR Clonase® Enzyme mix of (Life Technologies) by following the manufacturer's instructions. The product of this reaction was transformed into *E. coli* DH5α and transformants were selected for on LB Kan^{100} plates. Colonies were screened by colony PCR using the primers Ubi-exp and P_{PpMAX2}_◄. Plasmid from a single positively screened colony was isolated, linearised by *Sfi*I digestion, and used to transform WT *P. patens* as described. After selecting for stable $G418^{50}$ resistant colonies, the remaining colonies were screened by Phire PCR using the Ubi-exp and P_{PpMAX2}_◄ primers. The positive colonies, designated *P_{PpMAX2}:GUS*, were used for subsequent histochemical analysis to determine GUS localisation.

Results

The putative MAX2 homologue

A search for homologues of the *Arabidopsis* MAX2 (At4g42620) in the Phytozome version 9 database produced nine entries from the *Arabidopsis thaliana* database and 16 of the *Physcomitrella patens v1.6* database as hits for Phytozome's all-against-all Smith-Waterman alignment of protein sequences. However, only a single entry, Pp1s148_40v6, was more similar to AtMAX2 than the closest homolog from *Arabidopsis*, At4g15475 (Table 2). As the best candidate for this purpose, we designated the Pp1s148_40v6 locus as *PpMAX2* for the purposes of this study.

Table 2. **Homologues for AtMAX2 from *A. thaliana* and *P. patens v1.6* databases**

Subject ID	Score	Similarity	Identity	Coverage	*E*-value
Pp1s148_40v6	1551	58.6%	41.4%	99.7%	4.0E-108
Pp1s262_28v6	179	14.9%	8.2%	34.5%	2.0E-06
At4g15475	171	15.3%	9.5%	32.8%	1.0E-05
Pp1s364_6v6	163	8.4%	5.5%	15.9%	1.4E-05
At5g23340	163	14.7%	8.1%	33.8%	3.90E-05

A multiple sequence alignment was run using Clustal2.1 (Larkin et al., 2007) of the PpMAX2 sequence, the characterised sequences of AtMAX2, OsD3, PsRMS4, PhMAX2A, DgMAX2A and PtrMAX2A, from *Arabidopsis*, rice, pea, petunia, chrysanthemum and poplar respectively (Stirnberg et al., 2002; Ishikawa and Maekawa, 2005; Johnson et al., 2006; Drummond et al., 2012; Dong et al., 2013; Czarnecki et al., 2014), and of the putative MAX2 sequences, SmMAX2A and PsiMAX2, from *Selaginella moellendorfii* and *Picea sitchensis* (Delaux et al., 2012). Global alignment was accomplished with the selected set of sequences (Fig. 4). A major subset (165 aa) of the total translated PpMAX2 sequence (830 aa), ranging from A467 to V631, did not align with any of the sequences. However, variability does not appear to be uncommon for this region, even among the other sequences aligned.

Figure 4. Multiple sequence alignment of MAX2 orthologues. From top to bottom, the sequences used are AtMAX2, PtrMAX2A, PsRMS4, PhMAX2A, DgMAX2A, OsD3, SmMAX2A, PpMAX2 and PsiMAX2.

Subcellular localisation of recombinant GFP:PpMAX2 in *P. patens* protonemal cells

To determine the subcellular localisation of PpMAX2, a ZmUbi1:mGFP6:PpMAX2 construct was generated in the pMP1335 vector (see appendix H) and transformed into *P. patens*. The pMP1335 vector contains sequence to target the neutral locus Pp108 (Schaefer and Zrÿd, 1997) for homologous recombination. Three lines survived selection on G418[50], however, the *mGFP6:PpMAX2* sequence could only be amplified from lines 1 and 3. Line 1, *GFP:PpMAX2*, was subsequently selected for determining subcellular PpMAX2 localisation. Confocal imaging of protonemal tissue of *GFP:PpMAX2*, stained by Hoescht33342, a DNA specific stain that is nuclear localised, indicated that the recombinant GFP:PpMAX2 protein localises to the nucleus (Fig. 5).

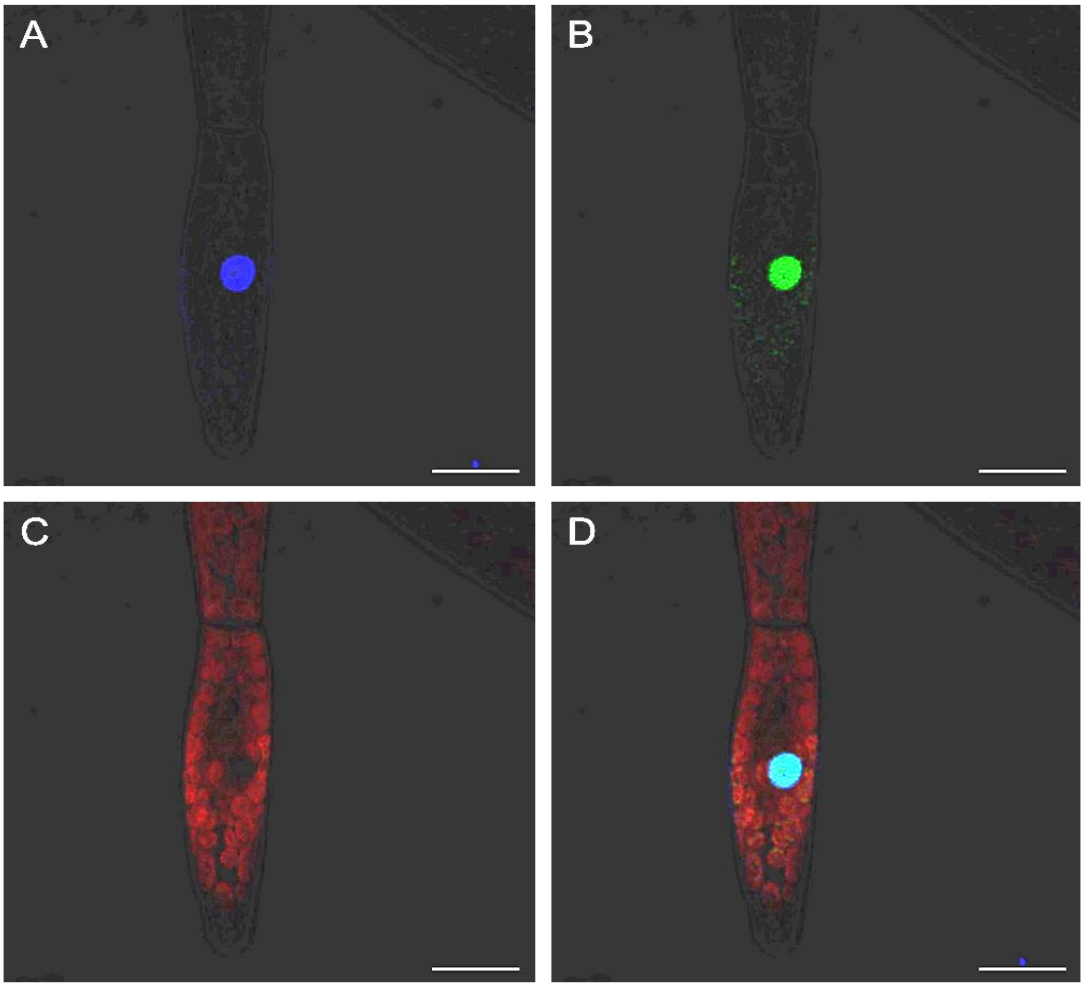

Figure 5. Subcellular localisation of recombinant *mGFP6:PpMAX2* in a protonemal tip cell. Hoescht33342 is localised to the nucleus (A). GFP fluorescence (B). Chloroplast autofluorescence (C). Superimposition of the images reveals co-localisation of Hoescht33342 and GFP to the nucleus (D). Scale bar = 20 µm.

Spatial distribution of P_{PpMAX2} regulated GUS expression

The pMP1300 vector is generally suitable for the generation and expression of GUS-fused proteins, however, to employ it as a tool for gene-promoter analysis, it was necessary to remove the native ZmUbi1 promoter. To this end, the vector pMP1301 was created by amplifying the entire pMP1300 vector - with the exclusion of the ZmUbi1 promoter. The P_{PpMAX2} sequence was subsequently cloned into the pMP1301 vector to generate the P_{PpMAX2}:GUS construct (see appendix G). The pMP1301:P_{PpMAX2} vector was transformed into WT *P. patens* and two transgenic lines were recovered. GUS expression was localised to gametophore tissue (*Fig.* 6) and could not be detected in protonemal tissue for both lines (*Fig.* 7). GUS expression was not detected in the rhizoid tissue.

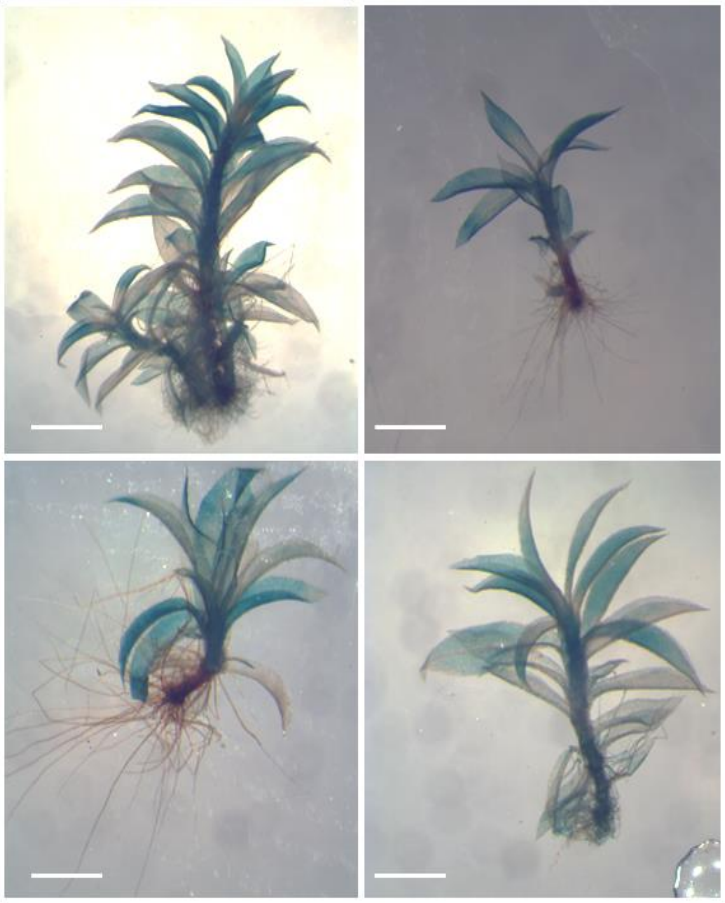

Figure 6. Spatial distribution of P_{PpMAX2} driven GUS expression. GUS is localised to the stem and leaf tissue of gametophores. GUS expression is absent from the rhizoids. Scale bar = 1mm.

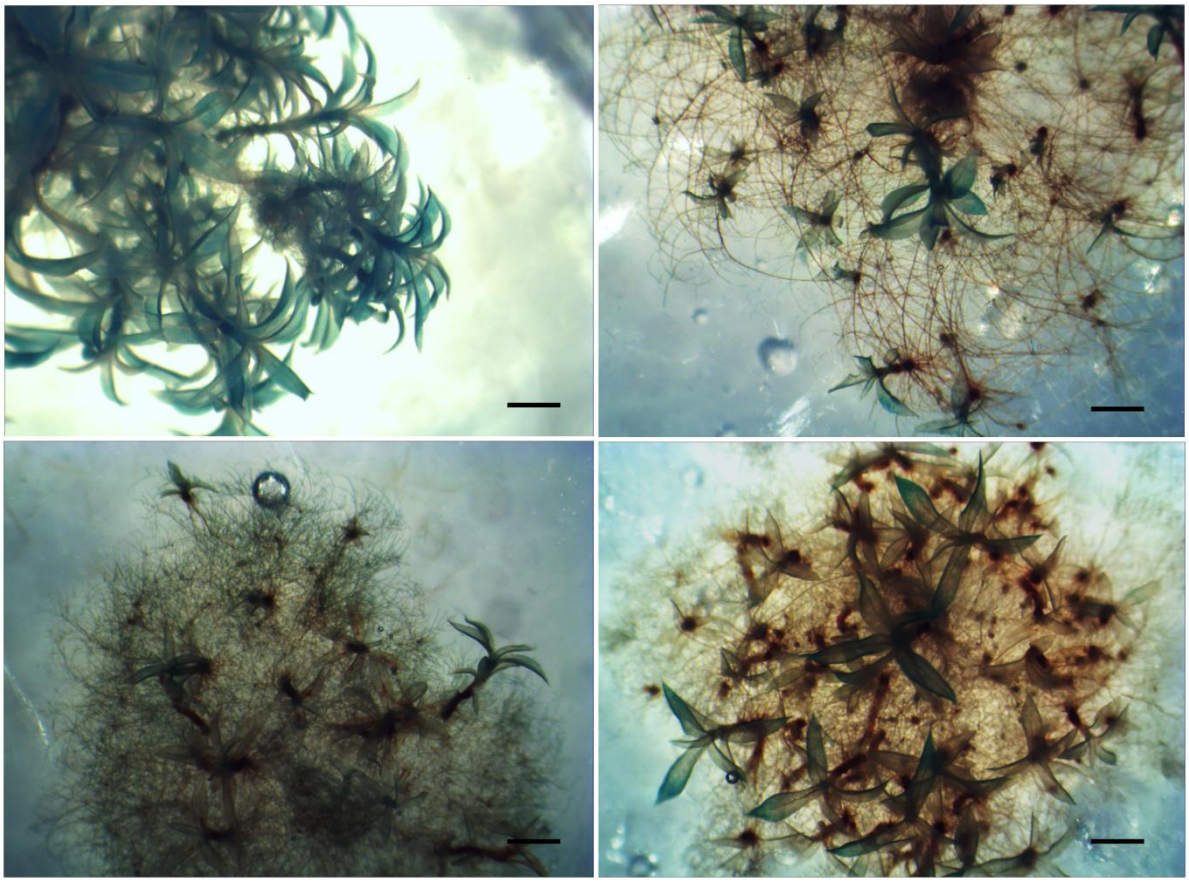

Figure 7. Spatial distribution of P_{PpMAX2} driven GUS expression in whole colonies. No GUS expression could be observed in protonema or rhizoids, however clear expression was detected in the leafy shoots. Scale bar = 1 mm.

The *Ppmax2::* lines display a novel phenotype

To generate mutants of the *PpMAX2* gene, two related constructs, p*Ppmax2-nptII*-KO1 and p*Ppmax2-hph*-KO1, were created and transformed into WT *P. patens*. After several transformations, 9 lines of the *nptII* construct, and 5 of the *hph* construct were recovered. Phire PCR was performed directly on plant tissue using the PpMAX2_scr primers. The primers were designed to bind to the regions bordering the locus targeted for homologous recombination. For the WT locus, a 2645 bp fragment (71+2493+81 bp) was expected to amplify. Due to the liberation of a 177 bp fragment during the generation of the KO1 constructs and the subsequent introduction of the antibiotic cassettes (±1500-1600 bp), stable transformants were expected to generate fragments of approximately 4000 bp for both the Ppmax2-*nptII*-KO1 and Ppmax2-*hph*-KO1 transformed lines. Of the 9 lines that maintained G418 resistance, colonies 6, 7, 8 and 9 conclusively genotyped as *Ppmax2::* mutants (Fig. 8). The fourth colony yielded multiple bands, likely from sample contamination.

Only one colony that maintained hygromycin resistance was genotyped as a *Ppmax2::* mutant (10). Multiple bands were amplified from colony 14, leaving the genotype inconclusive, and amplification from the remaining colonies (12, 13 and 15) failed altogether.

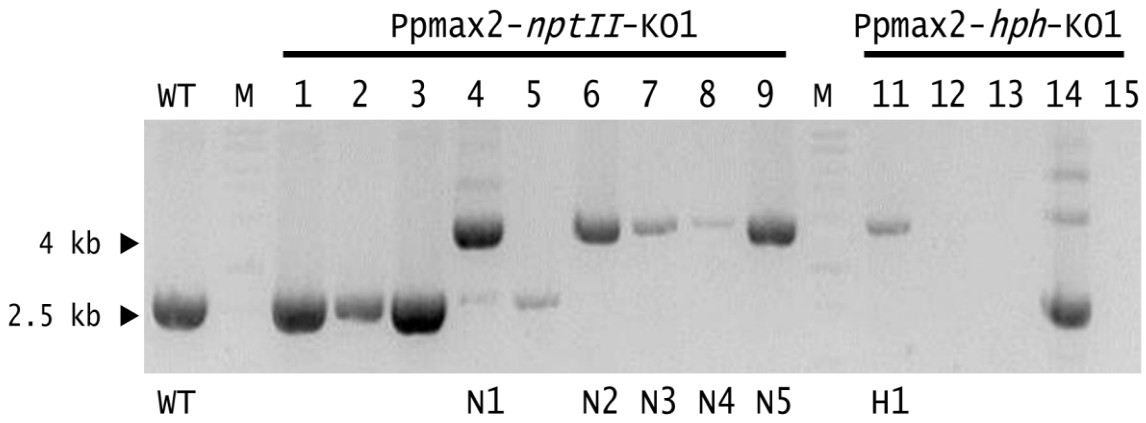

Figure 8. Genotyping of lines transformed with the Ppmax2-*nptII*-KO1 and Ppmax2-*hph*-KO1 constructs. A band corresponding to amplification from a recombined *PpMAX2* locus (±4 kb) was attained for colonies 4, 6, 7, 8, 9, 11 and 14. Fragments from colonies 1, 2, 3, 4, 5 and 14 corresponded to the 2.5 kb band generated by the WT control. Lines 4, 6, 7, 8, 9 and 11 were renamed as illustrated at the bottom of the image. M = BenchTop 1kb DNA Ladder (Promega)

The lines 4, 6, 7, 8 and 9 were subsequently renamed N1 to N5 and line 11 was renamed H1. All the lines that were genotyped as *Ppmax2::* mutants exhibited a distinctive phenotype (Fig. 9). The line N3 was chosen as representative for the *Ppmax2::* lines; therefore, all references made to *Ppmax2::* refer to this line specifically.

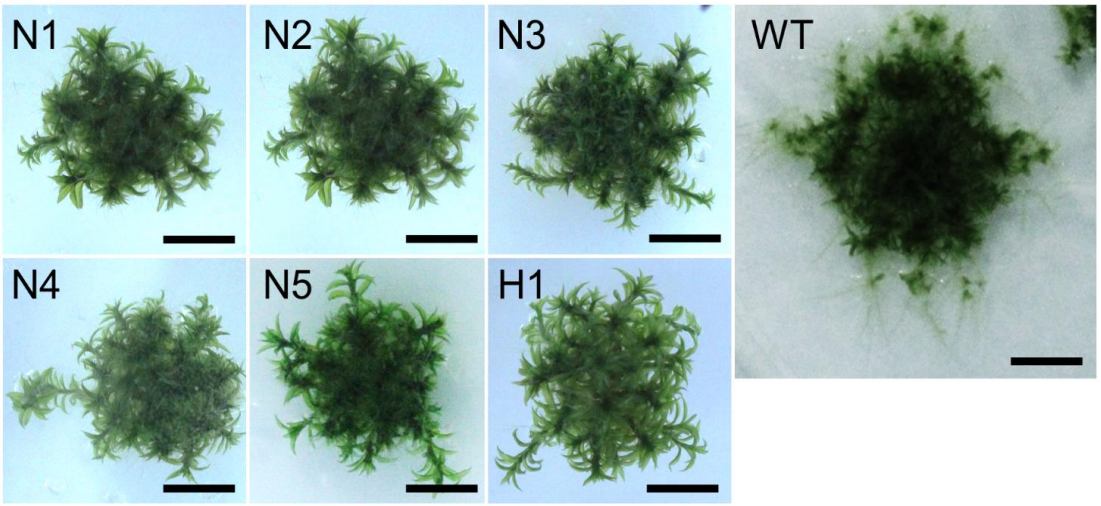

Figure 9. Phenotypes of colonies that were genotyped as *Ppmax2::* mutants. Scale bar = 5 mm.

When compared to the PpWT and *Ppccd8Δ* lines, the *Ppmax2::* line exhibited an apparent inability to produce protonemal tissue. To compare the differences in growth between the PpWT, *Ppccd8Δ* and *PPmax2::* lines, we first tried to isolated protoplasts from every line, however, the experiment was thwarted by the distinctive lack of protonemal tissue from the *Ppmax2::* lines, as protoplast isolations for *P. patens* are predominantly carried out from newly regenerated protonemal tissue of approximately 7 days old. The predominant tissue type exhibited by the *Ppmax2::* line was gametophore tissue. It was observed that an excess of 10^6 protoplasts could be isolated from the PpWT and *Ppccd8Δ* lines from tissue collected from 4 plates, however, up to 10 plates were required to isolate approximately 10^3 to 10^4 protoplasts for the *Ppmax2::* line.

The *Ppmax2::* mutants appeared to produce almost exclusively gametophores. Comparatively, the gametophores of the *Ppmax2::* line had fewer leaves per length of gametophore (Fig. 10) than the PpWT or *Ppccd8Δ* lines, suggesting that the *Ppmax2::* line has longer internodes than WT or *Ppccd8Δ*.

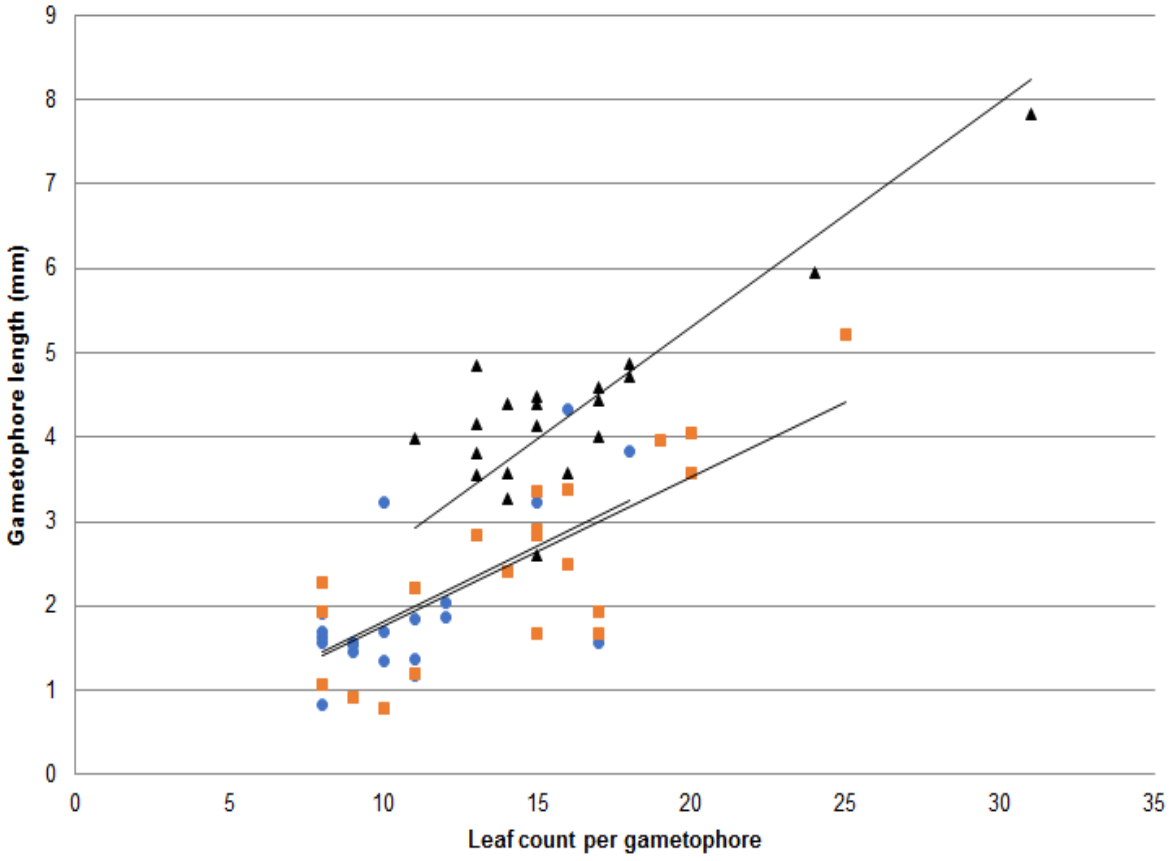

Figure 10. Leaf distribution on gametophores of *P. patens* lines. Correlation of the amount leafs counted per length of gametophore for the PpWT (●), *Ppccd8Δ* (■), and *Ppmax2::* (▲) lines. Linear trendlines intercept [0;0] and (from top to bottom) represent *Ppmax2::* (R^2 = 0.65), PpWT (R^2 = 0.44) and *Ppccd8Δ* (R^2 = 0.64)

The p*Ppmax2*-KO2 constructs

Multiple transformations were performed with the p*Ppmax2*-KO1 constructs, initially to no avail. We suspected at first that the constructs themselves could be the reason for this failure, and resolved to design a construct(s) that met the parameters for gene targeting, as outlined by Kamisugi et al. (2005). To that end, a new construct was generated, by employing overlap-extension PCR methodologies (Bryksin and Matsumura, 2010), that was composed of >1000 bp of flanking sequence for both the 5' and 3' regions of the *PpMAX2* gene (appendix F). Furthermore, the KO2 constructs were designed to knock out the entire coding sequence of the PpMAX2 gene, whereas the KO1 constructs would only disrupt the gene by insertion. To generate the KO2 construct, the entire locus, which includes 1000 bp of flanking sequence on both the 5'-region (upstream of start codon) and 3'-region (downstream of stop codon), was amplified. This 4686 bp product was used as template to amplify ±1000 bp of modified sequences for both flanking regions. The chimeric primer PpMAX2Δ_5'◄ adds sequence to the 1169 bp 5'-flanking region that is complementary to the 5'-end of the 3'-flanking region. Conversely, the PpMAXΔ_3'► primer adds base pairs to the 1008 bp 3'-flanking region complementary to the 3'-end of the 5'-flanking region. By combining these primers as template in a PCR utilising the PpMAX2Δ_5'► and PpMAX2Δ_3'◄ primers, the modified ends of the two fragments annealed and allowed for the amplification of a ±2000 bp fragment, composed solely of flanking sequences (see Fig. 11). Additionally, modifications within the chimeric ends of the overlapping primers introduced an *Stu*I restriction site, convenient for inserting any blunt-ended DNA. After the ±2000 bp *PpMAX2*flanks sequence was cloned into pJET1.2/blunt, the antibiotic cassettes were cloned into this introduced site to produce the p*Ppmax2-nptII*-KO2 and p*Ppmax2-hph*-KO2 constructs respectively.

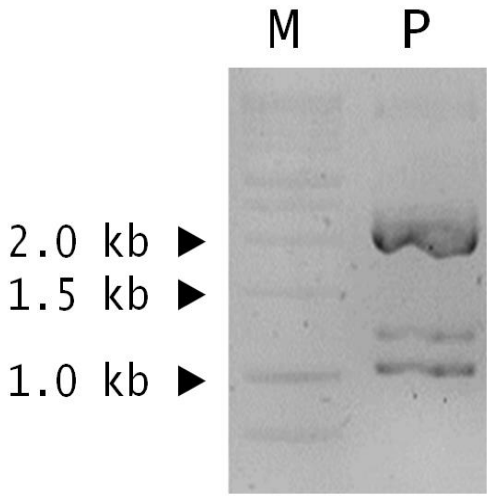

Figure 11. OE-PCR product(s). A ±2000 bp product (lane P, top) was amplified through OE-PCR by combining modified 5'-flanking (1169 bp) and 3'-flanking (1008 bp) sequences as template (bottom two bands). M = BenchTop 1kb DNA Ladder (Promega)

The *Ppccd8Δ Ppmax2Δ* double mutant resembles the *Ppmax2::* lines

Attempts to generate single *Ppmax2Δ* lines by transforming PpWT with the p*Ppmax2-nptII*-KO2 and p*Ppmax2-hph*-KO2 constructs respectively had not resulted in the recovery of any lines at the time of writing. However, following transformation of *Ppccd8Δ* protoplasts with the Ppmax2-*hph*-KO2 construct, five lines that maintained hygromycin resistance were recovered. All five lines were screened by Phire PCR using the PpMAX2Δ_scr primers. The primers bind to regions flanking the sequence targeted for homologous recombination and were therefore expected to amplify a 5683 bp fragment for the *PpMAX2* locus and approximately 4.5-4.6 bp for a recombined *Ppmax2Δ* locus. Only colony 3 generated a PCR fragment indicative of the modified locus (Fig. 12). Furthermore, the colony representing this line displayed the distinctive protonema-deficient phenotype that characterised the *Ppmax2::* lines, whereas the remaining colonies produced the dense protonema characteristic of the *Ppccd8Δ* mutant.

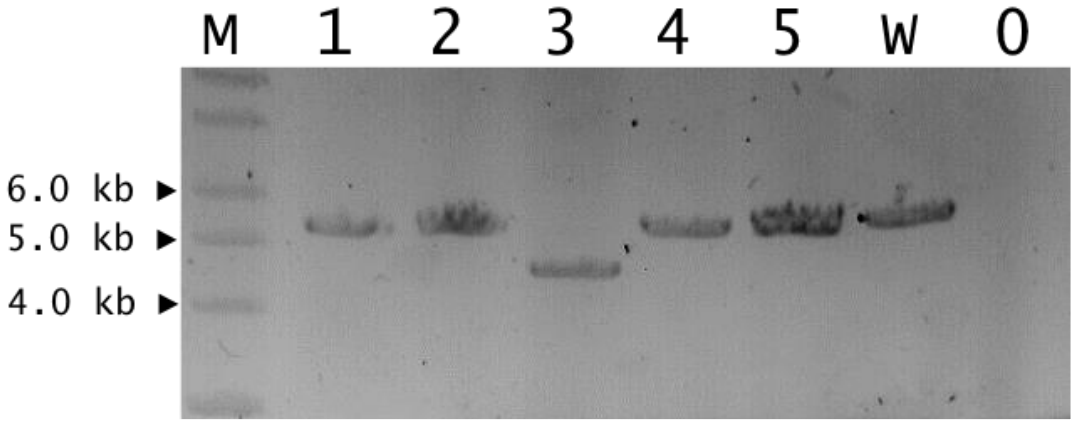

Figure 12. Genotyping of putative *Ppccd8Δ max2Δ* lines. Five colonies were regenerated from *Ppccd8Δ* protoplasts that had been transformed with the p*Ppmax2-hph*-KO2 construct. Colonies 1, 2, 4 and 5 genotyped as still having the WT locus. A smaller, <5 kb band was amplified from colony 3. M = BenchTop 1kb DNA Ladder (Promega). W = WT control. 0 = negative control.

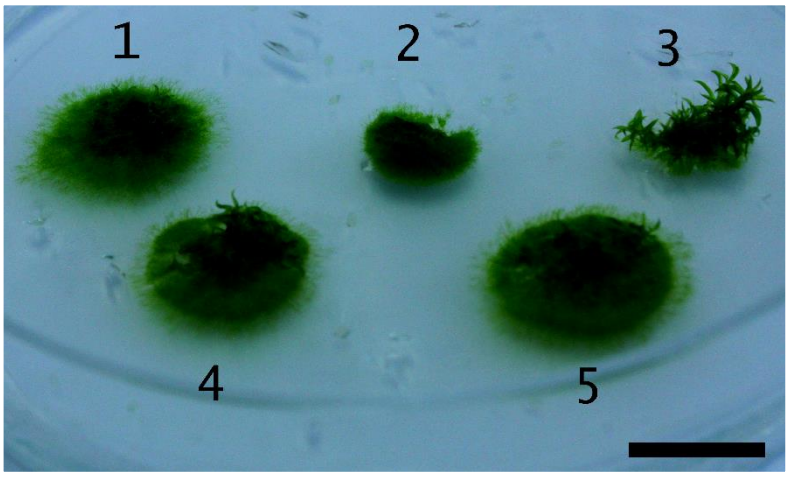

Figure 13. Phenotypes of regenerated *Ppccd8Δ* colonies from protoplasts transformed with the p*Ppmax2-hph*-KO2 construct. Colony 3 displays a prononema-deficient phenotype. Scale bar = 1 cm.

GR24 response of lines PpWT, *Ppccd8Δ* and *Ppmax2::*

GR24 response of the PpWT and *Ppccd8Δ* lines has previously been described and similar trends in regards to colony expansion were observed under our experimental setup (Proust et al., 2011). Exogenous strigolactones, introduces as 10^{-6} M GR24 to the growth medium, caused a visible reduction in the colony expansion of the PpWT and *Ppccd8Δ* lines, however, no such response was observed for the protonema-deficient *Ppmax2::* line.

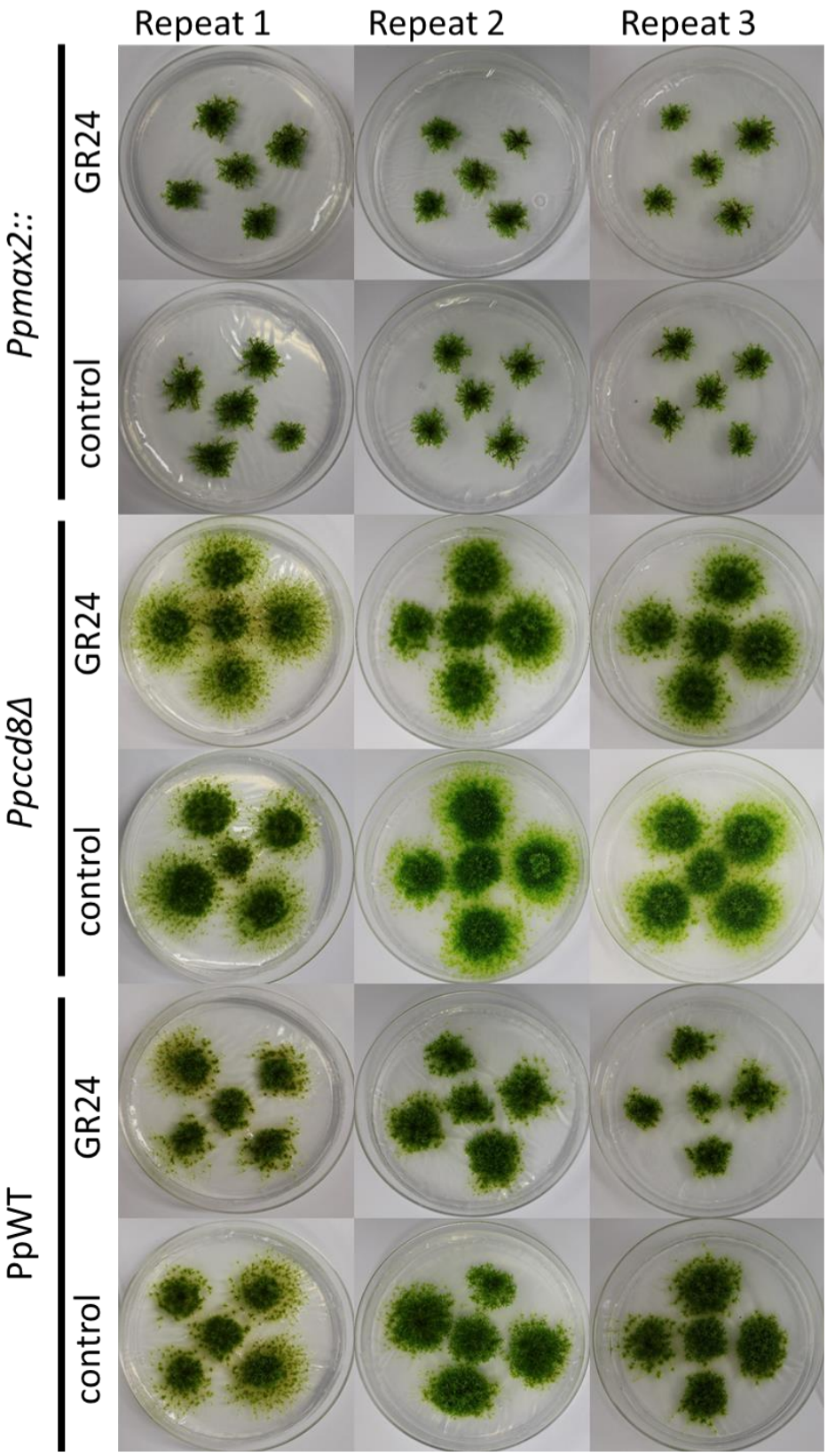

Figure 14. GR24 response of the PpWT, *Ppccd8Δ* and *Ppmax2::* lines after 40±2 days of treatment. By supplementing the growth medium with 10^{-6} M GR24, an inhibition of colony expantion was observed for the PpWT and *Ppccd8Δ* lines compared to the control plates. No such response was observed for the *Ppmax2::* line. Five individual colonies were spotted on each plate, with the 4 outside colonies being spaced exactly 2.5 cm apart.

Discussion

The alignment of the *PpMAX2* sequence to characterised *MAX2* sequences shows clear similarity. No other sequence from the *P. patens* genome aligns sufficiently to warrant placement within the *MAX2* clade of orthologues, leaving the *PpMAX2* as the primary, and probably only candidate for a *MAX2* homologue. A major fragment within the *PpMAX2* sequence does not align with the other *MAX2* proteins, and though the sequence within this region seems to be predisposed to variance - even among the *MAX2* orthologues from higher plants - the additional 165 amino acids could be indicative of novel functioning within bryophytes.

As F-box proteins, the MAX2 proteins form the substrate-recognising subunits of greater SCF-complexes. SCF-complexes tag target proteins for 26S-proteosomal degradation (Smalle and Vierstra, 2004). AtMAX2 has previously been shown to localise to (Shen et al., 2007; Stirnberg et al., 2007) and, more recently, to target proteins within the nucleus (Wang et al., 2013). Here we show that PpMAX2 is also localised to the nucleus. Although the nuclear localisation of PpMAX2 agrees with previous research, these findings should not be considered as conclusive evidence that *PpMAX2* is a functional homolog of the characterised *MAX2s*, as other F-box proteins have also been shown to localise to the nucleus (Dill et al., 2004; Vierstra, 2009).

In their original studies of branching mutants in pea, Beveridge et al. (1994-2000) were able to unknowingly identify several components of the strigolactone biosynthesis and signalling pathways, purely by studying the shared phenotypes of the *rms* lines: the increased bud outgrowth. Similar methods led to the discovery of the *max* mutants for *Arabidopsis* and the *d* mutants in rice. Therefore, the observation that mutations of certain key components of the strigolactone pathways reflect the same phenotype within their species has not only been key to strigolactone research in general, but is a key factor that underlies much of the biosynthesis, perception and signalling model for strigolactone research as we know it. We have therefore come to expect that mutants of strigolactone biosynthesis should exhibit a phenotype that would be reflected in the signalling mutants. Further characterisation as either biosynthetic or signalling mutant would subsequently rely on the response of these analogues mutants to exogenous strigolactone application. Our results demonstrate that these expectations are not realised within *P. patens*: where the *Ppccd8Δ* mutation results in an increase in colony expansion, primarily in the form of unchecked protonemal growth, the *Ppmax2::* mutant appeared to be incapable of producing protonema. The majority of the biomass in the *Ppmax2::* mutant was dedicated to producing leafy shoots.

Initially these confounding results led us to speculate that the *Ppmax2::* mutation, as an insertional mutation, might not have resulted in the complete abolishment of *PpMAX2* functions, but that it could have altered or enhanced the protein's functioning. However, a comparison of the relative positions of *max2/rms4/d3* mutations has convinced us that this is probably not the case (*Fig.* 15). The relative positions of the *max2-1* and *max2-2* mutations of *Arabidopsis*, the *rms4-7* and *rms4-8* mutations of pea and the *d3* mutation of rice are all downstream of the site targeted for insertion by the KO1 constructs. Furthermore, in *max2-4*, a SALK T-DNA insertion lies in a similar position within the *MAX2* gene and, as an insertion mutant, *max2*-4 is broadly analogous to *Ppmax2::*. As further substantive evidence, the double mutant, *Ppccd8Δ max2Δ*, of which the entire *PpMAX2* coding sequence has been deleted, exhibits the same protonema-deficient phenotype. We are therefore convinced that the *Ppmax2::* mutation results in a novel phenotype. We are still in the process of generating a single, *Ppmax2Δ* mutant, however, the *Ppmax2::* mutant lines have proven sufficient to produce a number of surprising results.

The fact that the double mutation *Ppccd8Δ Ppmax2Δ* results in the same protonema-deficient phenotype as is observed in *Ppmax2::* indicates that the product of *PpMAX2* expression overrides the function of *PpCCD8*. This does not give any indication of whether *PpMAX2* acts upstream or downstream of *PpCCD8*-dependant strigolactone biosynthesis, however, the nuclear localisation of PpMAX2, together with its homology to other F-box proteins, suggests that, should it act upstream of *PpCCD8*, it would exact strong feedback regulation; alternatively, should it act downstream of *PpCCD8*, it acts either in opposition to strigolactone biosynthesis, or its influence on moss development completely overrides that of *PpCCD8*. For either of these hypotheses to be proven or disproven, knowledge of the endogenous strigolactone levels within the *Ppmax2::* and *Ppccd8Δ max2Δ* lines will be vital. Our preliminary findings based on sqRT-PCR indicate that *PpCCD8* transcript levels might be up-regulated in *Ppmax2::* compared to PpWT (*results not shown*), hinting to a possible feedback regulation by *PpMAX2* action. However, due to the major differences in phenotypes of the lines tested, we have not yet been able to repeat the results on either uniform protonema or uniform leafy-shoot tissue samples from the *Ppmax2::* and PpWT lines.

The *Ppmax2::* line's lack of protonema also makes it difficult to draw a conclusion from the GR24 treatment experiments. While no effect on the *Ppmax2::* line's phenotype was noticed upon GR24 treatment (as was seen for the PpWT and *Ppccd8Δ* lines), it should be noted that the results of Proust et al. (2011) were mostly drawn from strigolactone responses observed in protonemal tissue. Therefore, to demonstrate that *Ppmax2::* is not strigolactone responsive, the GR24 responsiveness of protonemal tissue of the *Ppmax2::* lines will have to

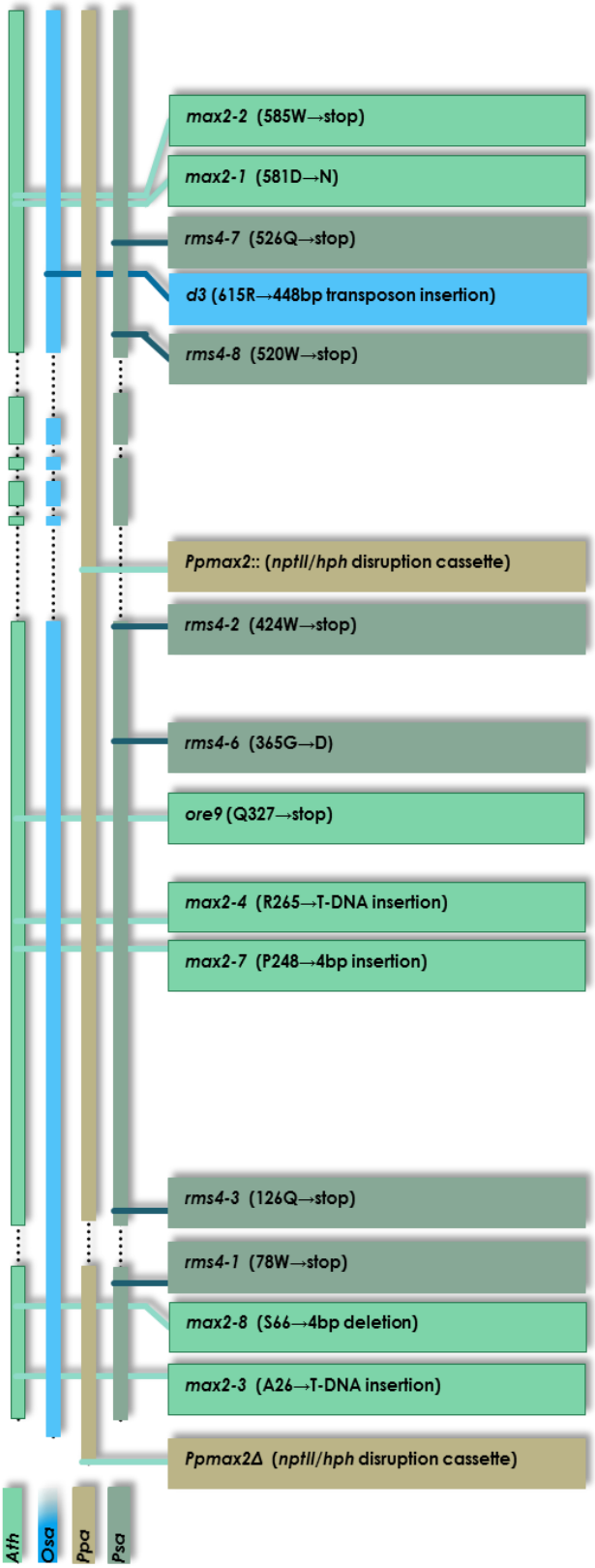

Figure 15. Relative positions of *max2/rms4/d3* mutations. A ClustalW alignment of the respective *Arabidopsis* (*Ath*, 693 aa), rice (*Osa*, 720 aa), *Physcomitrella* (*Ppa*, 830 aa) and pea (*Psa*, 708) protein sequences was manually converted to a representative figure and characterised mutations were mapped to their relative positions on the aligned sequences. The *Ppmax2::* mutation is relatively located upstream of the *max2-1, max2-2, rms4-7, rms4-8* and *d3* mutations.

be shown. A possible solution to these shortcomings that we intend to pursue is the regeneration of gametophyte tissue from either spores or protoplasts. Our preliminary experiments indicate that isolating protoplasts from the *Ppmax2::* lines is far more difficult than doing so from either the PpWT or *Ppccd8Δ* lines and that very few of these protoplasts are able to regenerate.

Our results indicate that *PpMAX2* might be involved in tissue differentiation, however, to conclude that *PpMAX2* directly regulates the differentiation of gametophore tissue to protonema would at this point amount to little more than conjecture. The phenotype observed could potentially be the consequence of a disturbance in a related pathway of which strigolactone is not the predominant effector, whereby *PpMAX2* could either function as a key component or it could extend influence through feedback regulation. By stating that *PpMAX2* regulates gametophore to protonema development, a segregation is created between the strigolactone biosynthesis pathway in *P. patens*, as was characterised through the studies of the *Ppccd8Δ* mutant (Proust et al., 2011; Hoffmann et al., 2014), and the yet to be clarified mechanism that implicates *PpMAX2*. The similarity of the PpMAX2 sequence to known MAX2 sequences indicates that it probably arose from a common, ancestral MAX2; the knowledge of *MAX2*-mediated regulation of strigolactone perception and signalling should not lightly be disregarded, even though it is difficult to reconcile the current model for the strigolactone pathway and the observed phenotypes. Nevertheless, this does leave room for alternative models of perception and signalling. The P_{PpMAX2}-determined localisation of *GUS* expression to predominantly gametophore tissue could potentially be explained in a model where *PpMAX2* dictates gametophore tissue dedifferentiation to protonema: by localising to the gametophore, *PpMAX2* is available to exact dedifferentiation to protonema should the signal be supplied. Alternatively, or perhaps additionally, *PpMAX2* could dictate whether the gametophore buds that arise in the protonema grow out to produce leafy shoots. Should this be the case, it would imply that the role for *PpMAX2* is broadly analogous to that of *AtMAX2*, and similar proteins in higher plants, as an inhibitor of bud outgrowth.

The transition from a haploid phase-dominated lifecycle to a diploid phase-dominated lifecycle, as characterised in bryophytes and tracheophytes respectively, certainly demanded many innovations of the ancestral species, however, far fewer genes were acquired for this transition than anticipated (Banks et al., 2011). This is understandable, as mosses are often defined by what they lack when compared to flowering plants. When one considers the attributes possessed by bryophytes, such as embryophyte-specific cell wall components, including lignin-precursors chemicals (Ligrone et al., 2008; Popper and Tuohy, 2010; Hörnblad et al., 2013), water-conducting cells (Ligrone et al., 2000) and major gene-

components of phytohormone pathways (Rensing et al., 2008) one can account for many phenotypic differences being the result of under-developed pathways. Furthermore, differences in the regulation of gene expression, as reflected in the transcript profiles of bryophytes compared to tracheophytes, gives evidence that many genes that were adapted within haploid-bodied bryophyte ancestors could be recruited during the developmental overhaul to a lifecycle dominated by a diploid body (Nishiyama et al., 2003; O'Donoghue et al., 2013). It is possible that the functions of *PpMAX2*, or even the strigolactone pathway in moss, might not resemble their counterparts as we know them in higher plants.

To assess the homology of *PpMAX2* to particularly *AtMAX2*, attempts have been made to introduce the *PpMAX2* gene into the *Atmax2* background (data not shown). We have not yet been able to characterise the *PpMAX2* gene as a true functional homologue of the *A. thaliana MAX2*, as we have only been able to generate a single *Atmax2::PpMAX2* line to date. The phenotype of this single line does not suggest complete functional complementation, however, these findings were omitted as more lines are needed for any valid conclusions to be drawn. Even though *PpMAX2* might not be a functional homologue for *AtMAX2*, it might still be a participant of hormone signalling in *P. patens*.

Previous studies of the gibberellin pathway in *P. patens* have indicated that, although the pathway might not be complete as it has been described in higher plants, the basal components that are present do assert some function (Hirano et al., 2007; Yasumura et al., 2007; Anterola et al., 2009). *P. patens* is able to produce *ent*-kaurene, a gibberellin precursor that is required for spore germination (Anterola et al., 2009). Precursors of GID1 and DELLA proteins, key components of gibberellin signalling in higher plants, are also found in the *P. patens* proteome, however, whether these proteins exert true functional similarity to their homologues in higher plants still needs to be conclusively proven (Hirano et al., 2007; Yasumura et al., 2007; Schwechheimer and Willige, 2009). The recent finding that the α/β-fold hydrolase, D14, and the DELLA protein, SLR1, from rice are able to interact (Nakamura et al., 2013), suggests that, by only looking for conservation or divergence of characterised hormonal pathways only, one risks overlooking interactions that might not be quite as apparent, such as the ever-complex cross-talks between hormone pathways. It is noteworthy that *P. patens* does not have any *D14* sequences in its genome and, though *D14-like* sequences have been found, these have only been characterised as receptors for smoked-derived karrikins (Hoffmann et al., 2014).

From the results of this study we cannot conclusively determine whether *PpMAX2* represents a true functional homolog of characterised *MAX2s*, but the data suggests strongly that it represents an ancestral version of those F-box proteins. The knowledge that we have

of the various components of the strigolactone pathway and the way in which those components interact would dictate that the phenotype of *Ppmax2::* and *Ppccd8Δ max2Δ* should reflect that of *Ppccd8Δ*, however, from our findings, that clearly is not the case. Our observations that *Ppmax2::* does not respond to strigolactone could be due to a response(s) being masked by the severely protonema-deficient phenotype of the various *Ppmax2* mutants that we have generated. It is still not known whether *PpMAX2* could functionally complement *Atmax2*, and only by doing so will it be clear whether *PpMAX2* shares any of its functions with orthologues *MAX2s* from higher plants. Whether *PpMAX2* has any role to play in the strigolactone pathway is still to be determined and it would be interesting to discover which proteins or metabolites directly interact with *PpMAX2.*

Future prospects

Future works will include more attempts at recovering *Atmax2::PpMAX2* lines and, reciprocally, we intend to introduce *AtMAX2* into a *Ppmax2* background. The phenotype of the *Ppmax2::* line does not lend itself to homologous recombination as it is difficult to generate protoplasts for transformation, however, by introducing the *AtMAX2* gene into a PpWT background prior to targeting the *PpMAX2* locus for knock-out transformation, complementation could be achieved, or at least attempted, in *P. patens*.

Although the *Ppmax2::* line has proven invaluable in this study, we have not yet been able generate spores from it. We suspect that the *Ppmax2::* line has become sterile as a result of prolonged periods of vegetative propagation (Collier and Hughes, 1982; Cove et al., 2009). We have since attained spores of the PpWT line and are making progress towards generating a *Ppmax2Δ* single mutant from freshly germinated tissue. By using the KO2 constructs we hope to circumvent any potential scepticism or confusion that could arise in regards to the insertion mutation of *Ppmax2::* and the difference of this mutation to the *Ppmax2Δ* mutation that was introduced into the *Ppccd8Δ* background.

To obtain a more direct measure of the role *PpMAX2* has on the strigolactone pathway in *P. patens*, we would propose that the strigolactones exuded by the *Ppmax2::* (or *Ppmax2Δ*) and *Ppccd8Δ Ppmax2Δ* lines be measured by LC-MS/MS. Previous studies have shown that strigolactone biosynthesis is dependent on a feedback mechanism that probably originates from *MAX2* (Hayward et al., 2009). If *PpMAX2* truly is a *MAX2* homologue that partakes in this feedback mechanism, we would expect to see an increase in strigolactone levels in the *Ppmax2::* line as a result of the disrupted feedback mechanism. Alternatively, if *PpMAX2* has no relation to strigolactone regulation, we would expect to detect similar levels of strigolactones in the *Ppmax2::* background to what would be produced by PpWT. Additionally, an indirect transcriptomic approach could be pursued by RT-qPCR of known

strigolactone responsive genes, such as *PpCCD7* (Proust et al., 2011), on the PpWT, *Ppccd8Δ*, *Ppmax2::* (*Ppmax2Δ*) and *Ppccd8Δ max2Δ* lines. The response of *PpCCD7* expression should also be tested in regards to exogenous strigolactone application to these lines. Our current findings pertaining to *PpMAX2*-mediated regulation of tissue types suggests that it will also be worth looking at the expression levels of *PpMAX2* in gametophore tissue as compared to its expression levels in protonema by sqRT-PCR in the PpWT line as a supplement to the GUS histochemical assay.

In addition to analysing the regulation of strigolactone and strigolactone-regulated genes, future research should also extend to the analysis of specifically *PpMAX2*-related genes. As it is possible that *PpMAX2* is not the true functional homolog for the characterised *MAX2s*, and might therefore not be related to strigolactone signalling, it might be needed to first identify *PpMAX2*-related genes through a forward genetics approach. A mutagenized library of the *Ppmax2::* and *Ppccd8Δ* lines could be created through ethyl methanesulfonate (EMS) or UV-exposure. This approach could yield transcriptional regulators acting downstream of *PpMAX2*. Should this approach be feasible, the already detrimental phenotype attributed to the *Ppmax2* mutation could potentially facilitate in the recovery of affected mutant lines. However, for future works that entail forward-genetics, the ability to sexually outcross lines will be crucial, as mapping of the affected loci will need to be done for the research to bear any relevance. Optimising our methods for inducing sporophytogenesis will therefore take precedence.

The generation of spores should also allow us to more accurately determine the strigolactone response of the *Ppmax2::* line, specifically on a protonemal level, however, our preliminary findings indicate that it should be possible, though perhaps more difficult, to do so by using protoplasts.

If we were to describe a simple vegetative lifecycle of *P. patens* in culture, we could say that protonemal tissue develops to produce gametophore buds; the gametophore buds subsequently grow out to produce gametophores; the gametophores could then be used to start a fresh culture of protonema. It is evident that this cycle has been skewed to favour predominantly gametophore growth in the *Ppmax2::* line. To determine whether the phenotype of *Ppmax2::* is due to the line being unable to dedifferentiate from gametophores to protonema, an observation of regenerating tissue from a *Ppmax2::* leaf-tip cutting, over time, should be revealing. By observing the regeneration of a *Ppmax2::* protoplast to a mature gametophore should also tell if *PpMAX2* extends its influence to the development or outgrowth of gametophore buds.

Literature Cited

Akiyama K, Matsuzaki K, Hayashi H (2005) Plant sesquiterpenes induce hyphal branching in arbuscular mycorrhizal fungi. Nature **435**: 824–827

Alder A, Holdermann I, Beyer P, Al-Babili S (2008) Carotenoid oxygenases involved in plant branching catalyse a highly specific conserved apocarotenoid cleavage reaction. The Biochemical Journal **416**: 289–296

Alder A, Jamil M, Marzorati M, Bruno M, Vermathen M, Bigler P, Ghisla S, Bouwmeester H, Beyer P, Al-Babili S (2012) The path from β-carotene to carlactone, a strigolactone-like plant hormone. Science **335**: 1348–1351

Allsopp A, Mitra GC (1958) The morphology of protonema and bud formation in the Bryales. Annals of Botany **22**: 95–115

Anterola A, Shanle E, Mansouri K, Schuette S, Renzaglia K (2009) Gibberellin precursor is involved in spore germination in the moss *Physcomitrella patens*. Planta **229**: 1003–1007

Arite T, Umehara M, Ishikawa S, Hanada A, Maekawa M, Yamaguchi S, Kyozuka J (2009) *D14*, a strigolactone-insensitive mutant of rice, shows an accelerated outgrowth of tillers. Plant & Cell Physiology **50**: 1416–1424

Ashton NW, Cove DJ, Featherstone DR (1979) The isolation and physiological analysis of mutants of the moss, *Physcomitrella patens*, which over-produce gametophores. Planta **144**: 437–442

Banks JA, Nishiyama T, Hasebe M, Bowman JL, Gribskov M, dePamphilis C, Albert VA, Aono N, et al. (2011) The *Selaginella* genome identifies genetic changes associated with the evolution of vascular plants. Science **332**: 960–963

Bartels PG, Watson CW (1978) Inhibition of carotenoid synthesis by fluridone and norflurazon. Weed Science **26**: 198–203

Beveridge C, Ross J, Murfet I (1996) Branching in pea (action of genes *Rms3* and *Rms4*). Plant Physiology **110**: 859–865

Beveridge C, Symons G, Murfet I (1997a) The *rms1* mutant of pea has elevated indole-3-acetic acid levels and reduced root-sap zeatin riboside content but increased branching controlled by graft-transmissible signal(s). Plant Physiology **115**: 1251–1258

Beveridge CA, Murfet IC, Kerhoas L, Sotta B, Miginiac E, Rameau C (1997b) The shoot controls zeatin riboside export from pea roots. Evidence from the branching mutant *rms4*. The Plant Journal **11**: 339–345

Beveridge CA, Ross JJ, Murfet IC (1994) Branching mutant *rms-2* in *Pisum sativum* (grafting studies and endogenous indole-3-acetic acid levels). Plant Physiology **104**: 953–959

Beveridge CA, Symons GM, Turnbull CGN (2000) Auxin inhibition of decapitation-induced branching is dependent on graft-transmissible signals regulated by genes *Rms1* and *Rms2*. Plant Physiology **123**: 689–698

Booker J, Auldridge M, Wills S, McCarty D (2004) *MAX3*/*CCD7* is a carotenoid cleavage dioxygenase required for the synthesis of a novel plant signaling molecule. Current Biology **14**: 1232–1238

Brown R, Greenwood A, Johnson A, AG L (1951) The stimulant involved in the germination of *Orobanche minor* Sm. 1. Assay technique and bulk preparation of the stimulant. Biochemical Journal **48**: 559–564

Brown R, Johnson AW, Robinson E, Todd AR (1949) The stimulant involved in the germination of *Striga hermonthica*. Proceedings of the Royal Society of London Series B, Biological Sciences **136**: 1–12

Brown R, Johnson AW, Robinson E, Tyler GJ (1952) The *Striga* germination factor. 2. Chromatographic purification of crude concentrates. Biochemical Journal **50**: 596–600

Brundrett MC (2002) Coevolution of roots and mycorrhizas of land plants. New Phytologist **154**: 275–304

Bryksin AV, Matsumura I (2010) Overlap extension PCR cloning: a simple and reliable way to create recombinant plasmids. BioTechniques **48**: 463–465

Butler LG (1994) Chemical communication between the parasitic weed *Striga* and its crop host: a new dimension in allelochemistry. *In* Inderjit, KMM Dakshini, FA Einhellig, eds, Allelopathy. American Chemical Society, Washington, DC, pp 158–168

Cardoso C, Zhang Y, Jamil M, Hepworth J, Charnikhova T, Dimkpa SON, Meharg C, Wright MH, et al. (2014) Natural variation of rice strigolactone biosynthesis is associated with the deletion of two *MAX1* orthologs. Proceedings of the National Academy of Sciences **111**: 2379–2384

Challis RJ, Hepworth J, Mouchel C, Waites R, Leyser O (2013) A role for *more axillary growth1* (*MAX1*) in evolutionary diversity in strigolactone signaling upstream of *MAX2*. Plant Physiology **161**: 1885–1902

Chevalier F, Nieminen K, Sánchez-Ferrero JC, Rodríguez ML, Chagoyen M, Hardtke CS, Cubas P (2014) Strigolactone promotes degradation of DWARF14, an α/β hydrolase essential for strigolactone signaling in *Arabidopsis*. The Plant Cell **26**: 1134–1150

Collier PA, Hughes KW (1982) Life cycle of the moss, *Physcomitrella patens*, in culture. Journal of tissue culture methods **7**: 19–22

Cook C, Whichard L, Turner B, Wall M, Egley G (1966) Germination of witchweed (*Striga lutea* Lour.): isolation and properties of a potent stimulant. Science **154**: 1189–1190

Cook C, Whichard L, Wall M, Egley GH, Coggon P, Luhan PA, McPhail A (1972) Germination stimulants. II. Structure of strigol, a potent seed germination stimulant for witchweed (*Striga lutea*). Journal of the American Chemical Society **1447**: 6198–6199

Cove D, Knight D (1993) The moss *Physcomitrella patens*, a model system with potential for the study of plant reproduction. The Plant Cell **5**: 1483–1488

Cove DJ, Kammerer W, Knight CD, Leech MJ, Martin CR, Wang TL (1990) Developmental genetic studies of the moss, *Physcomitrella patens*. Symposia of the Society for Experimental Biology **45**: 31–43

Cove DJ, Perroud P-F, Charron AJ, McDaniel SF, Khandelwal A, Quatrano RS (2009) The moss *Physcomitrella patens*: a novel model system for plant development and genomic studies. Cold Spring Harbor Protocols **2009**: 69–104

Czarnecki O, Yang J, Wang X, Wang S, Muchero W, Tuskan G, Chen J-G (2014) Characterization of *MORE AXILLARY GROWTH* genes in Populus. PLoS one **9**: e102757

Delaux P-M, Xie X, Timme RE, Puech-Pages V, Dunand C, Lecompte E, Delwiche CF, Yoneyama K, Bécard G, Séjalon-Delmas N (2012) Origin of strigolactones in the green lineage. The New Phytologist **195**: 857–871

Dill A, Thomas SG, Hu J, Steber CM, Sun T (2004) The *Arabidopsis* F-Box Protein SLEEPY1 targets gibberellin signaling repressors for gibberellin-induced degradation. The Plant Cell **16**: 1392–1405

Dolby LJ, Hanson G (1976) Convenient synthesis of a hydrindan precursor to strigol. The Journal of Organic Chemistry **41**: 563–564

Dong L, Ishak A, Yu J, Zhao R, Zhao L (2013) Identification and functional analysis of three *MAX2* orthologs in chrysanthemum. Journal of Integrative Plant Biology **55**: 434–442

Drummond RSM, Sheehan H, Simons JL, Martínez-Sánchez NM, Turner RM, Putterill J, Snowden KC (2012) The expression of petunia strigolactone pathway genes is altered as part of the endogenous developmental program. Frontiers in Plant Science. doi: 10.3389/fpls.2011.00115

Edwards K, Johnstone C, Thompson C (1991) A simple and rapid method for the preparation of plant genomic DNA for PCR analysis. Nucleic Acids Research **19**: 1349

Engel PP (1968) The induction of biochemical and morphological mutants in the moss *Physcomitrella patens*. American Journal of Botany **55**: 438–446

Gaiji N, Cardinale F, Prandi C, Bonfante P, Ranghino G (2012) The computational-based structure of Dwarf14 provides evidence for its role as potential strigolactone receptor in plants. BMC Research Notes **5**: 307

Gomez-Roldan V, Fermas S, Brewer PB, Puech-Pagès V, Dun E, Pillot J-P, Letisse F, Matusova R, et al. (2008) Strigolactone inhibition of shoot branching. Nature **455**: 189–194

Goodstein DM, Shu S, Howson R, Neupane R, Hayes RD, Fazo J, Mitros T, Dirks W, et al. (2011) Phytozome: a comparative platform for green plant genomics. Nucleic Acids Research doi: 10.1093/nar/gku990

Grimsley NH, Ashton NW, Cove DJ (1977a) Complementation analysis of auxotrophic mutants of the moss, *Physcomitrella patens*, using protoplast fusion. Molecular & General Genetics **155**: 103–107

Grimsley NH, Ashton NW, Cove DJ (1977b) The production of somatic hybrids by protoplast fusion in the moss, *Physcomitrella patens*. Molecular & General Genetics **154**: 97–100

Gross D (1975) Growth regulating substances of plant origin. Phytochemistry **14**: 2105–2112

Hamiaux C, Drummond RSM, Janssen BJ, Ledger SE, Cooney JM, Newcomb RD, Snowden KC (2012) DAD2 is an α/β hydrolase likely to be involved in the perception of the plant branching hormone, strigolactone. Current Biology **22**: 2032–2036

Hauck C, Müller S, Schildknecht H (1992) A germination stimulant for parasitic flowering plants from *Sorghum bicolor*, a genuine host plant. Journal of Plant Physiology **139**: 474–478

Hayward A, Stirnberg P, Beveridge C, Leyser O (2009) Interactions between auxin and strigolactone in shoot branching control. Plant Physiology **151**: 400–412

Heather JB, Mittal RSD, Sih CJ (1974) Total synthesis of d1-strigol. Journal of the American Chemical Society **96**: 1976–1977

Heather JB, Mittal RSD, Sih CJ (1976) Synthesis of the witchweed seed germination stimulant (+)-strigol. Journal of the American Chemical Society **98**: 3661–3669

Hirano K, Nakajima M, Asano K, Nishiyama T, Sakakibara H, Kojima M, Katoh E, Xiang H, et al. (2007) The GID1-mediated gibberellin perception mechanism is conserved in the Lycophyte *Selaginella moellendorffii* but not in the Bryophyte *Physcomitrella patens*. The Plant Cell **19**: 3058–3079

Hiwatashi Y, Fujita T, Sato Y, Tanahashi T, Nishiyama T, Sakakibara K, Kofuji R, Aono N, et al. (2008) PHYSCOmanual version1.4. http://www.nibb.ac.jp/evodevo/PHYSCOmanual/00Eindex.htm (accessed December 2014)

Hoffmann B, Charlot F (2009) Transformation of the moss *Physcomitrella patens*. SGAP, INRA, Versailles

Hoffmann B, Proust H, Belcram K, Labrune C, Boyer F-D, Rameau C, Bonhomme S (2014) Strigolactones inhibit caulonema elongation and cell division in the moss *Physcomitrella patens*. PLoS one **9**: e99206

Hohe A, Rensing SA, Mildner M, Lang D, Reski R (2002) Day length and temperature strongly influence sexual reproduction and expression of a novel MADS-box gene in the moss *Physcomitrella patens*. Plant Biology **4**: 595–602

Hörnblad E, Ulfstedt M, Ronne H, Marchant A (2013) Partial functional conservation of IRX10 homologs in *Physcomitrella patens* and *Arabidopsis thaliana* indicates an evolutionary step contributing to vascular formation in land plants. BMC Plant Biology **13**: 3

Hosokawa Z, Shi L, Prasad TK, Cline MG (1990) Apical dominance control in *Ipomoea nil*: the influence of the shoot apex, leaves and stem. Annals of Botany **65**: 547–556

Ishikawa S, Maekawa M (2005) Suppression of tiller bud activity in tillering *dwarf* mutants of rice. Plant Cell Physiology **46**: 79–86

Jiang L, Liu X, Xiong G, Liu H, Chen F, Wang L, Meng X, Liu G, et al. (2013) DWARF 53 acts as a repressor of strigolactone signalling in rice. Nature **504**: 401–405

Johnson AW, Gowada G, Hassanali A, Knox J, Monaco S, Razavi Z, Rosebery G (1981) The preparation of synthetic analogues of strigol. Journal of the Chemical Society, Perkin Transactions **1**: 1734

Johnson AW, Rosebery G, Parker C (1976) A novel approach to *Striga* and *Orobanche* control using synthetic germination stimulants. Weed Research **16**: 223–227

Johnson X, Brcich T, Dun E, Goussot M, Haurogné K, Beveridge C, Rameau C (2006) Branching genes are conserved across species. Genes controlling a novel signal in pea are coregulated by other long-distance signals. Plant Physiology **142**: 1014–1026

Kamisugi Y, Cuming A, Cove D (2005) Parameters determining the efficiency of gene targeting in the moss *Physcomitrella patens*. Nucleic Acids Research **33**: 1–10

Kohlen W (2011) Regulation of biosynthesis and transport of strigolactones and their effect on plant development. PhD thesis, Wageningen University, The Netherlands

Koltai H (2014) Receptors, repressors, PINs: a playground for strigolactone signaling. Trends in Plant Science In press

Larkin MA, Blackshields G, Brown NP, Chenna R, McGettigan PA, McWilliam H, Valentin F, Wallace IM, et al. (2007) Clustal W and Clustal X version 2.0. Bioinformatics **23**: 2947–2948

Leyser O (2003) Regulation of shoot branching by auxin. Trends in Plant Science **8**: 541–545

Ligrone R, Carafa A, Duckett JG, Renzaglia KS, Ruel K (2008) Immunocytochemical detection of lignin-related epitopes in cell walls in bryophytes and the charalean alga *Nitella*. Plant Systematics & Evolution **270**: 257–272

Ligrone R, Ducket JG, Renzaglia KS (2000) Conducting tissues and phyletic relationships of bryophytes. Philosophical Transactions of the Royal Society of London **355**: 795–813

Lin H, Wang R, Qian Q, Yan M, Meng X, Fu Z, Yan C, Jiang B, et al. (2009) DWARF27, an iron-containing protein required for the biosynthesis of strigolactones, regulates rice tiller bud outgrowth. The Plant Cell **21**: 1512–1525

Liu Y-C, Vidali L (2011) Efficient Polyethylene Glycol (PEG) Mediated Transformation of the moss *Physcomitrella patens*. Journal of Visualized Experiments. doi: 10.3791/2560

MacAlpine GA, Raphael RA, Shaw A, Taylor AW, Wild H-J (1974) Synthesis of the germination stimulant (±)-strigol. Journal of the Chemical Society, Chemical Communications 834–835

Macías FA, García-Díaz MD, Jorrín J, Galindo JCG (2006) Playing with chemistry: studies on *Orobanche* spp. Germination stimulants. *In* MJ Reigosa, N Pedrol, L González, eds, Allelopathy. Springer Netherlands, pp 495–510

Mangnus E, Dommerholt F, Jong RL de, Zwanenburg B (1992) Improved synthesis of strigol analog GR24 and evaluation of the biological activity of its diastereomers. Journal of Agriculture and Food Chemistry **8**: 1230–1235

Matusova R, Rani K (2005) The strigolactone germination stimulants of the plant-parasitic *Striga* and *Orobanche* spp. are derived from the carotenoid pathway. Plant Physiology **139**: 920–934

Morris S, Turnbull C (2001) Mutational analysis of branching in pea. Evidence That Rms1 and Rms5 regulate the same novel signal. Plant Physiology **126**: 1205–1213

Nakamura H, Xue Y, Miyakawa T, Hou F, Qin H, Fukui K, Shi X, Ito E, et al. (2013) Molecular mechanism of strigolactone perception by DWARF14. Nature Communications **4**: 2613

Nakosteen PC, Hughes KW (1978) Sexual life cycle of three species of Funariaceae in culture. The Bryologist **81**: 307–314

Napoli CA, Beveridge CA, Snowden KC (1999) Reevaluating concepts of apical dominance and the control of the axillary bud outgrowth. Current Topics in Developmental Biology **44**: 127–169

Nishiyama T, Fujita T, Shin-I T, Seki M, Nishide H, Uchiyama I, Kamiya A, Carninci P, et al. (2003) Comparative genomics of *Physcomitrella patens* gametophytic transcriptome and *Arabidopsis thaliana*: Implication for land plant evolution. Proceedings of the National Academy of Sciences **100**: 8007–8012

O'Donoghue M-T, Chater C, Wallace S, Gray JE, Beerling DJ, Fleming AJ (2013) Genome-wide transcriptomic analysis of the sporophyte of the moss *Physcomitrella patens*. Journal of Experimental Botany doi:10.1093/jxb/ert190

Oh SA, Park JH, Lee GI, Paek KH, Park SK, Nam HG (1997) Identification of three genetic loci controlling leaf senescence in *Arabidopsis thaliana*. The Plant Journal **12**: 527–535

Ongaro V, Leyser O (2008) Hormonal control of shoot branching. Journal of Experimental Botany **59**: 67–74

Pepperman AB, Connick WJ Jr., Vail SL, Worsham AD, Pavlista AD, Moreland DE (1982) Evaluation of precursors and analogs of strigol as witchweed (*Striga asiatica*) seed germination stimulants. Weed Science **30**: 561–566

Popper ZA, Tuohy MG (2010) Beyond the green: understanding the evolutionary puzzle of plant and algal cell walls. Plant Physiology **153**: 373–383

Prigge MJ, Lavy M, Ashton NW, Estelle M (2010) *Physcomitrella patens* auxin-resistant mutants affect conserved elements of an auxin-signaling pathway. Current Biology **20**: 1907–1912

Proust H, Hoffmann B, Xie X, Yoneyama K, Schaefer DG, Yoneyama K, Nogué F, Rameau C (2011) Strigolactones regulate protonema branching and act as a quorum sensing-like signal in the moss *Physcomitrella patens*. Development **138**: 1531–1539

Rani K, Zwanenburg B, Sugimoto Y, Yoneyama K, Bouwmeester HJ (2008) Biosynthetic considerations could assist the structure elucidation of host plant produced

rhizosphere signalling compounds (strigolactones) for arbuscular mycorrhizal fungi and parasitic plants. Plant Physiology & Biochemistry **46**: 617–626

Rensing SA, Lang D, Zimmer AD, Terry A, Salamov A, Shapiro H, Nishiyama T, Perroud P-F, et al. (2008) The *Physcomitrella* genome reveals evolutionary insights into the conquest of land by plants. Science **319**: 64–69

Reski R (1998) Development, genetics and molecular biology of mosses. Botanica Acta **111**: 1–15

Sambrook J, Russell DW (2001) Molecular cloning: a laboratory manual. CSHL Press

Satish K, Gutema Z, Grenier C, Rich PJ, Ejeta G (2012) Molecular tagging and validation of microsatellite markers linked to the *low germination stimulant* gene (*lgs*) for *Striga* resistance in sorghum [*Sorghum bicolor* (L.) Moench]. Theoretical & Applied Genetics **124**: 989–1003

Scaffidi A, Waters MT, Ghisalberti EL, Dixon KW, Flematti GR, Smith SM (2013) Carlactone-independent seedling morphogenesis in *Arabidopsis*. The Plant Journal **76**: 1–9

Schaefer DG, Zrÿd JP (1997) Efficient gene targeting in the moss *Physcomitrella patens*. The Plant Journal **11**: 1195–1206

Schmiedel G, Schnepf E (1980) Polarity and growth of caulonema tip cells of the moss *Funaria hygrometrica*. Planta **147**: 405–413

Schüßler A, Schwarzott D, Walker C (2001) A new fungal phylum, the Glomeromycota: phylogeny and evolution. Mycological Research **105**: 1413–1421

Schwacke R, Schneider A, Graaff E van der, Fischer K, Catoni E, Desimone M, Frommer WB, Flügge U-I, Kunze R (2003) ARAMEMNON, a novel database for *Arabidopsis* integral membrane proteins. Plant Physiology **131**: 16–26

Schwartz S, Qin X, Loewen M (2004) The biochemical characterization of two carotenoid cleavage enzymes from *Arabidopsis* indicates that a carotenoid-derived compound inhibits lateral branching. Journal of Biological Chemistry **279**: 46940–46945

Schwechheimer C, Willige BC (2009) Shedding light on gibberellic acid signalling. Current Opinion in Plant Biology **12**: 57–62

Seto Y, Sado A, Asami K, Hanada A, Umehara M, Akiyama K, Yamaguchi S (2014) Carlactone is an endogenous biosynthetic precursor for strigolactones. Proceedings of the National Academy of Sciences of the United States of America **111**: 1640–1645

Shen H, Luong P, Huq E (2007) The F-box protein MAX2 functions as a positive regulator of photomorphogenesis in *Arabidopsis*. Plant Physiology **145**: 1471–1483

Sironval C (1947) Expériences sur les stades de développement de la forme filamenteuse en culture de *Funaria hygrometrica* L. Bulletin de la Société Royale de Botanique de Belgique **79**: 48–78

Smalle J, Vierstra RD (2004) The ubiquitin 26S proteasome proteolytic pathway. Annual Review of Plant Biology **55**: 555–590

Sorefan K, Booker J (2003) *MAX4* and *RMS1* are orthologous dioxygenase-like genes that regulate shoot branching in *Arabidopsis* and pea. Genes & Development **17**: 1469–1474

Stirnberg P, Furner IJ, Ottoline Leyser HM (2007) MAX2 participates in an SCF complex which acts locally at the node to suppress shoot branching. The Plant Journal **50**: 80–94

Stirnberg P, Sande K van de, Leyser HMO (2002) *MAX1* and *MAX2* control shoot lateral branching in *Arabidopsis*. Development **129**: 1131–1141

Tamasloukht M, Séjalon-Delmas N, Kluever A, Jauneau A, Roux C, Bécard G, Franken P (2003) Root factors induce mitochondrial-related gene expression and fungal respiration during the developmental switch from asymbiosis to presymbiosis in the arbuscular mycorrhizal fungus *Gigaspora rosea*. Plant Physiology **131**: 1468–1478

Turnbull CGN, Booker JP, Leyser HMO (2002) Micrografting techniques for testing long-distance signalling in *Arabidopsis*. The Plant Journal **32**: 255–262

Umehara M, Hanada A, Yoshida S, Akiyama K, Arite T, Takeda-Kamiya N, Magome H, Kamiya Y, et al. (2008) Inhibition of shoot branching by new terpenoid plant hormones. Nature **455**: 195–200

Vierstra RD (2009) The ubiquitin-26S proteasome system at the nexus of plant biology. Nature Reviews Molecular Cell Biology **10**: 385–397

Wang Y, Sun S, Zhu W, Jia K, Yang H, Wang X (2013) Strigolactone/MAX2-induced degradation of brassinosteroid transcriptional effector BES1 regulates shoot branching. Developmental Cell **27**: 681–688

Waters MT, Brewer PB, Bussell JD, Smith SM, Beveridge CA (2012a) The Arabidopsis ortholog of rice *DWARF27* acts upstream of *MAX1* in the control of plant development by strigolactones. Plant Physiology **159**: 1073–1085

Waters MT, Nelson DC, Scaffidi A, Flematti GR, Sun YK, Dixon KW, Smith SM (2012b) Specialisation within the DWARF14 protein family confers distinct responses to karrikins and strigolactones in *Arabidopsis*. Development **139**: 1285–1295

Wettstein DF v (1924) Morphologie und physiologie des formwechsels der moose auf genetischer grundlage. I. Zeitschrift für Induktive Abstammungs- & Vererbungslehre **33**: 1–236

Woo H, Chung K, Park J, Oh S (2001) ORE9, an F-box protein that regulates leaf senescence in *Arabidopsis*. The Plant Cell **13**: 1779–1790

Worsham AD, Moreland DE, Klingman GC (1964) Characterization of the *Striga asiatica* (Witchweed) germination stimulant from *Zea mays* L. Journal of Experimental Botany **15**: 556–567

Xie X, Yoneyama K, Yoneyama K (2010) The strigolactone story. Annual Review of Phytopathology **48**: 93–117

Yasumura Y, Crumpton-Taylor M, Fuentes S, Harberd NP (2007) Step-by-step acquisition of the gibberellin-DELLA growth-regulatory mechanism during land-plant evolution. Current Biology **17**: 1225–1230

Zhao L-H, Zhou XE, Wu Z-S, Yi W, Xu Y, Li S, Xu T-H, Liu Y, et al. (2013) Crystal structures of two phytohormone signal-transducing α/β hydrolases: karrikin-signaling KAI2 and strigolactone-signaling DWARF14. Cell Research **23**: 436–439

Zhou F, Lin Q, Zhu L, Ren Y, Zhou K, Shabek N, Wu F, Mao H, et al. (2013) D14-SCF(D3)-dependent degradation of D53 regulates strigolactone signalling. Nature **504**: 406–410

Appendix A: List of Primers

Oligo name	Sequence (5' → 3')
PpMAX2_►	ATGGAAGCAGTGCAGTGG
PpMAX2_◄	TTAATCAGGAAAACCTCGTTTTGC
pJET1.2_►	CGACTCACTATAGGGAGAGCGGC
pJET1.2_◄	AAGAACATCGATTTTCCATGGCAG
PpMAX2_seq►1	ATTGTTAAGTTGGTGCGGTG
PpMAX2_seq►2	GAGCTGAGGTTGAAGAACTG
PpMAX2_seq►3	GGCCTTGGAAGTGGTAATTT
PpMAX2_seq◄1	AAATTACCACTTCCAAGGCC
PpMAX2_seq◄2	CAGTTCTTCAACCTCAGCTC
PpMAX2_seq◄3	CACCGCACCAACTTAACAAT
PpMAX2_scr►	GGCCTTCTTCGACATTATGC
PpMAX2_scr◄	GACAAGTAGCCGTGGTTTAC
PpMAX2Δ_5'►	GGGAGCTTCGGTTTGTAGC
PpMAX2Δ_5'◄	GCTACCCACGTATTCTTCGTAGGCCTGTCTTGCCTCTGCTACACC
PpMAX2Δ_3'►	GGTGTAGCAGAGGCAAGACAGGCCTACGAAGAATACGTGGGTAGC
PpMAX2Δ_3'◄	GGTATGTATGTGTGCAATCGC
PpMAX2Δ_scr►	GAGAGATTGTATTCCTTGCTTCC
PpMAX2Δ_scr◄	TATTGACTGCACCGTTGAAG
M13_►	GTTTTCCCAGTCACGAC
M13_◄	CAGGAAACAGCTATGAC
Ubipr	TAACTTAGACATGCAATGCTC
Ubi-exp	ATACGCTATTTATTTGCTTGG
GFP_►	AGATGGTGATGTTAATGGGC
P_{PpMAX2}_►	GAGGCTTTCGGTTACCGAG
P_{PpMAX2}_◄	GTCTTGCCTCTGCTACACC
P_{PpMAX2}_seq►	CCACTCATGCATGCATGC
P_{PpMAX2}_seq◄	GGTGGTCTCGCATCTCTC

The annealing temperatures for all the primers used were 58°C.

Appendix B: Map of locus Pp1s148_40v6

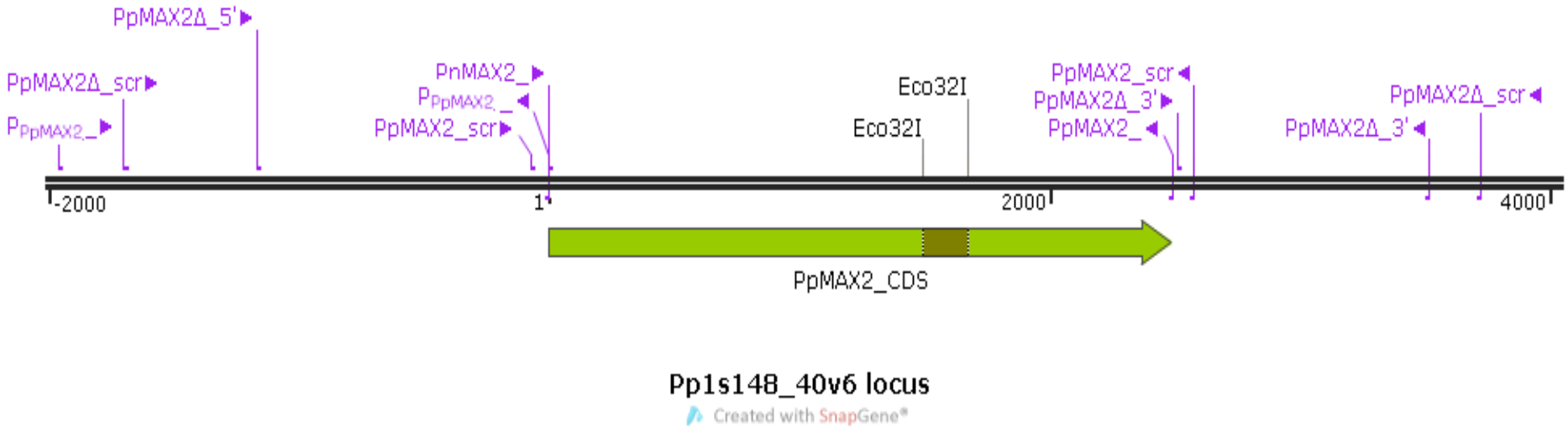

Appendix C: Map of pJET1.2::*PpMAX2*

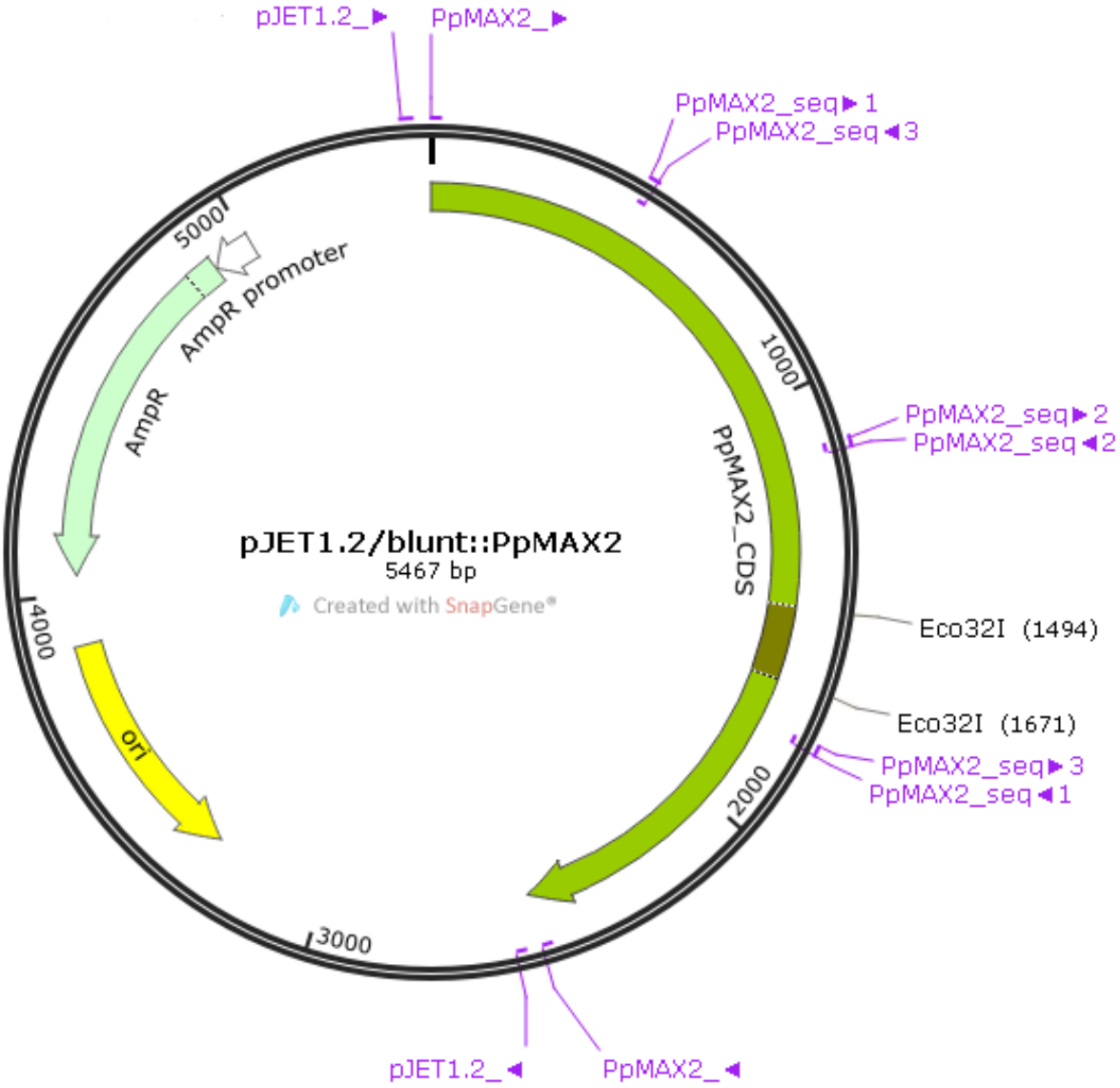

Appendix D: Map of p*Ppmax2-nptII*-KO1

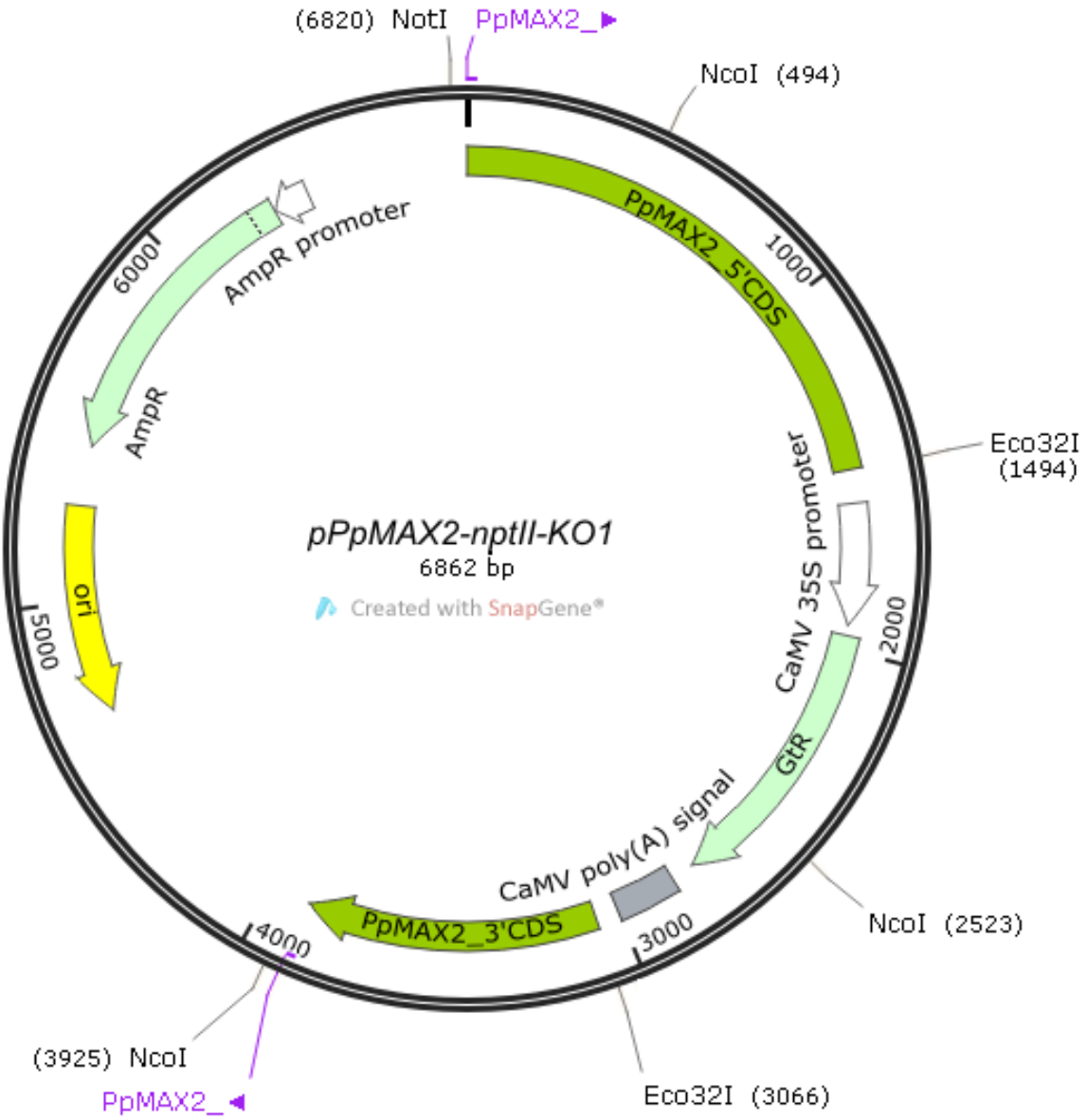

Appendix E: Illustration of OE-PCR templates

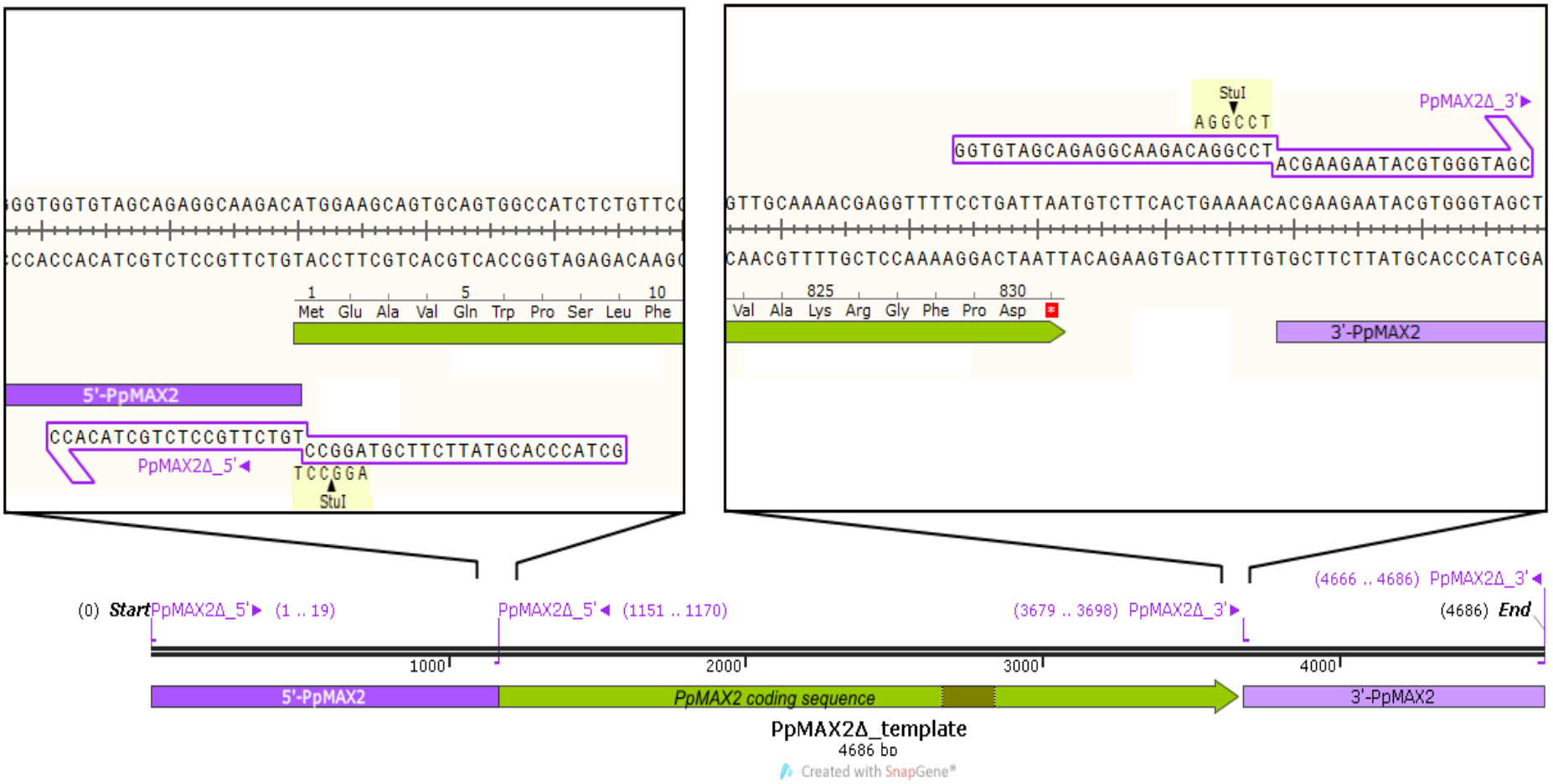

Appendix F: p*Ppmax2-nptII*-KO2

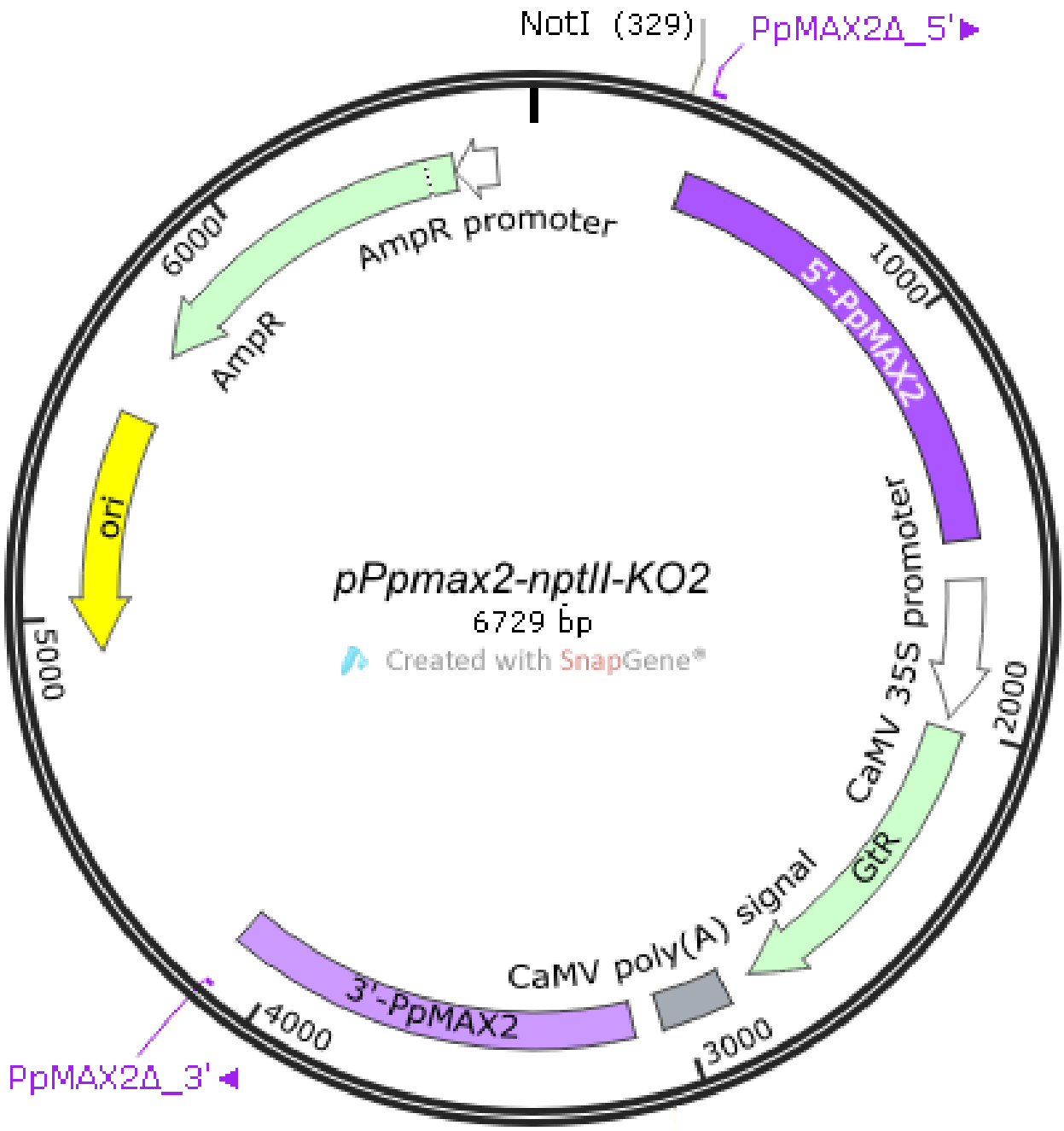

Appendix G: Map of pMP1301::P_{Ppmax2}

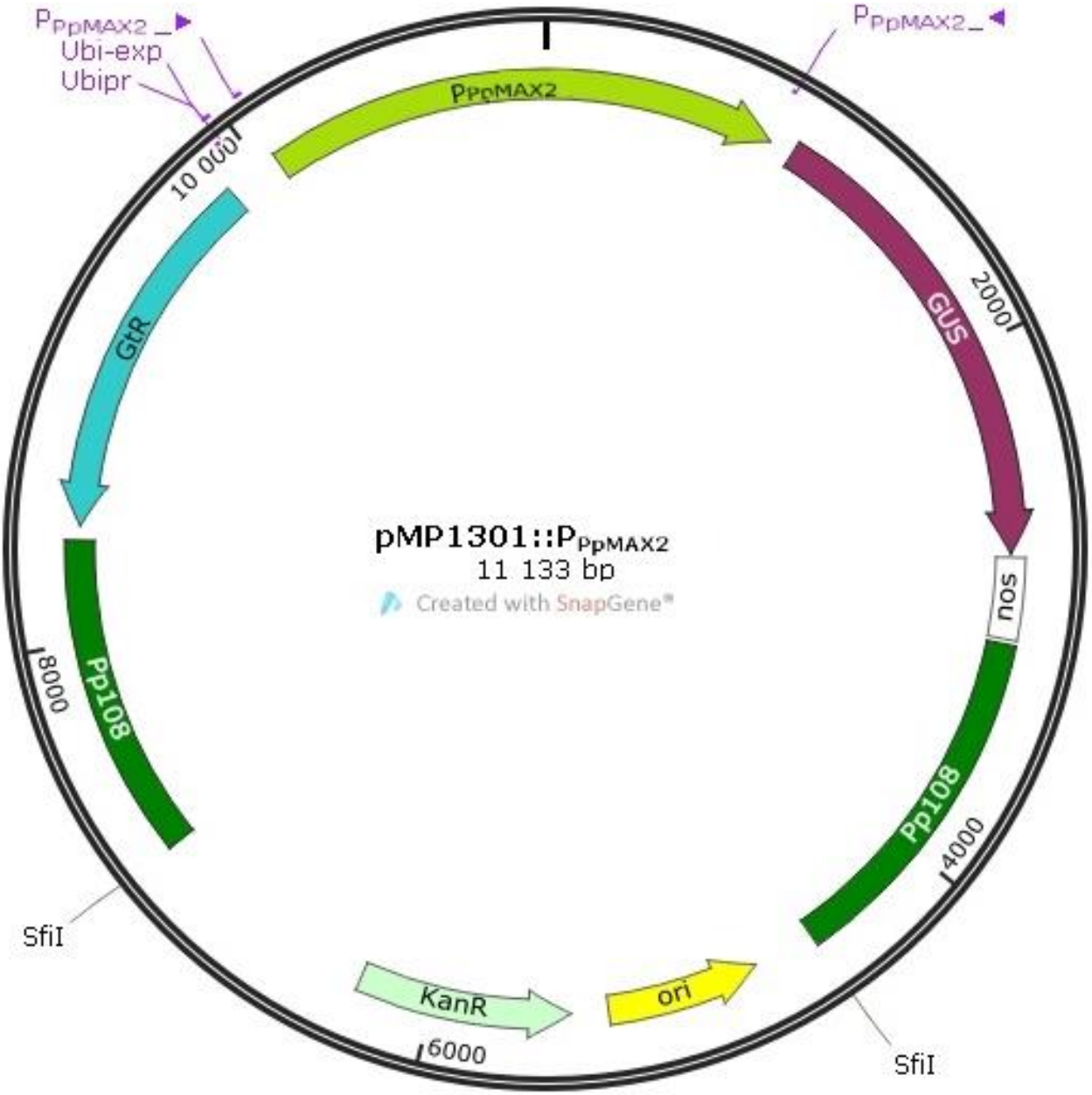

Appendix H: Map of pMP1335::*PpMAX2*